

## CO and O<sub>2</sub> Binding to Pseudo-tetradentate Ligand–Copper(I) Complexes with a Variable N-Donor Moiety: Kinetic/Thermodynamic Investigation Reveals Ligand-Induced Changes in Reaction Mechanism

Heather R. Lucas, Gerald J. Meyer,\* and Kenneth D. Karlin\*

*Department of Chemistry, The Johns Hopkins University, Baltimore, Maryland 21218*

Received May 20, 2010; E-mail: karlin@jhu.edu; meyer@jhu.edu

**Abstract:** The kinetics, thermodynamics, and coordination dynamics are reported for O<sub>2</sub> and CO 1:1 binding to a series of pseudo-tetradentate ligand–copper(I) complexes (<sup>D</sup>LCu<sup>I</sup>) to give Cu<sup>I</sup>/O<sub>2</sub> and Cu<sup>I</sup>/CO product species. Members of the <sup>D</sup>LCu<sup>I</sup> series possess an identical tridentate core structure where the cuprous ion binds to the bispicolylamine (L) fragment. <sup>D</sup>L also contains a fourth variable N-donor moiety {D = benzyl (Bz); pyridyl (Py); imidazolyl (Im); dimethylamino (NMe<sub>2</sub>); (*tert*-butylphenyl)pyridyl (TBP); quinolyl (Q)}. The structural characteristics of <sup>D</sup>LCu<sup>I</sup>–CO and <sup>D</sup>LCu<sup>I</sup> are detailed, with X-ray crystal structures reported for <sup>TBP</sup>LCu<sup>I</sup>–CO, <sup>Bz</sup>LCu<sup>I</sup>–CO, and <sup>Q</sup>LCu<sup>I</sup>. Infrared studies (solution and solid-state) confirm that <sup>D</sup>LCu<sup>I</sup>–CO possess the same four-coordinate core structure in solution with the variable D moiety “dangling”, i.e., not coordinated to the copper(I) ion. Other trends observed for the present series appear to derive from the degree to which the D-group interacts with the cuprous ion center. Electrochemical studies reveal close similarities of behavior for <sup>Im</sup>LCu<sup>I</sup> and <sup>NMe<sub>2</sub></sup>LCu<sup>I</sup> (as well as for <sup>TBP</sup>LCu<sup>I</sup> and <sup>Q</sup>LCu<sup>I</sup>), which relate to the O<sub>2</sub> binding kinetics and thermodynamics. Equilibrium CO binding data (*K*<sub>CO</sub>, Δ*H*<sup>‡</sup>, Δ*S*<sup>‡</sup>) were obtained by conducting UV–visible spectrophotometric CO titrations, while CO binding kinetics and thermodynamics (*k*<sub>CO</sub>, Δ*H*<sup>‡</sup>, Δ*S*<sup>‡</sup>) were measured through variable-temperature (193–293 K) transient absorbance laser flash photolysis experiments, λ<sub>ex</sub> = 355 nm. Carbon monoxide dissociation rate constants (*k*<sub>–CO</sub>) and corresponding activation parameters (Δ*H*<sup>‡</sup>, Δ*S*<sup>‡</sup>) have also been obtained. CO binding to <sup>D</sup>LCu<sup>I</sup> follows an associative mechanism, with the increased donation from D leading to higher *k*<sub>CO</sub> values. Unlike observations from previous work, the *K*<sub>CO</sub> values increased as the *k*<sub>CO</sub> and *k*<sub>–CO</sub> values declined; the latter decreased at a faster rate. By using the “flash-and-trap” method (λ<sub>ex</sub> = 355 nm, 188–218 K), the kinetics and thermodynamics (*k*<sub>O<sub>2</sub></sub>, Δ*H*<sup>‡</sup>, Δ*S*<sup>‡</sup>) for O<sub>2</sub> binding to <sup>NMe<sub>2</sub></sup>LCu<sup>I</sup> and <sup>Im</sup>LCu<sup>I</sup> were measured and compared to those for <sup>Py</sup>LCu<sup>I</sup>. A surprising change in the O<sub>2</sub> binding mechanism was deduced from the thermodynamic Δ*S*<sup>‡</sup> values observed, associative for <sup>Py</sup>LCu<sup>I</sup> but dissociative for <sup>NMe<sub>2</sub></sup>LCu<sup>I</sup> and <sup>Im</sup>LCu<sup>I</sup>; these results are interpreted as arising from a difference in the timing of electron transfer from copper(I) to O<sub>2</sub> as this molecule coordinates and a tetrahydrofuran (THF) solvent molecule dissociates. The change in mechanism was not simply related to alterations in <sup>D</sup>LCu<sup>I/II</sup> geometries or the order in which O<sub>2</sub> and THF coordinate. The equilibrium O<sub>2</sub> binding constant (*K*<sub>O<sub>2</sub></sub>, Δ*H*<sup>‡</sup>, Δ*S*<sup>‡</sup>) and O<sub>2</sub> dissociation rate constants (*k*<sub>–O<sub>2</sub></sub>, Δ*H*<sup>‡</sup>, Δ*S*<sup>‡</sup>) were also determined. Overall the results demonstrate that subtle changes in the coordination environment, as occur over time through evolution in nature or through controlled ligand design in synthetic systems, dictate to a critically detailed level the observed chemistry in terms of reaction kinetics, structure, and reactivity, and thus function. Results reported here are also compared to relevant copper and/or iron biological systems and analogous synthetic ligand–copper systems.

### Introduction

A detailed understanding of copper(II/I)–protein active site properties and their 1:1 small-molecule (CO, O<sub>2</sub>, NO, etc.) binding characteristics is of importance and has inspired a diverse array of research efforts for biochemists and synthetic bioinorganic chemists alike.<sup>1–6</sup> Research advances through

synthetic modeling have helped to gain important insights into copper coordination and reactivity through generation of ligands with precisely optimized formulations and through study of their ligand–copper/small-molecule chemistry. In this context, however, the ability to directly monitor the formation, structures, and subsequent reactivity of Cu<sup>I</sup>/O<sub>2</sub>-derived primary species, i.e., mononuclear copper(II)–superoxo complexes formulated

- (1) Kim, E.; Chufan, E. E.; Kamaraj, K.; Karlin, K. D. *Chem. Rev.* **2004**, *104*, 1077–1133.
- (2) Wasser, I. M.; de Vries, S.; Moenne-Loccoz, P.; Schroder, I.; Karlin, K. D. *Chem. Rev.* **2002**, *102*, 1201–1234.
- (3) Lucas, H. R.; Karlin, K. D. *Met. Ions Life Sci.* **2009**, *6*, 295–362.
- (4) Lewis, E. A.; Tolman, W. B. *Chem. Rev.* **2004**, *104*, 1047–1076.

- (5) Mirica, L. M.; Ottenwaelder, X.; Stack, T. D. P. *Chem. Rev.* **2004**, *104*, 1013–1045.
- (6) Solomon, E. I.; Szilagyi, R. K.; George, S. D.; Basumallick, L. *Chem. Rev.* **2004**, *104*, 419–458.

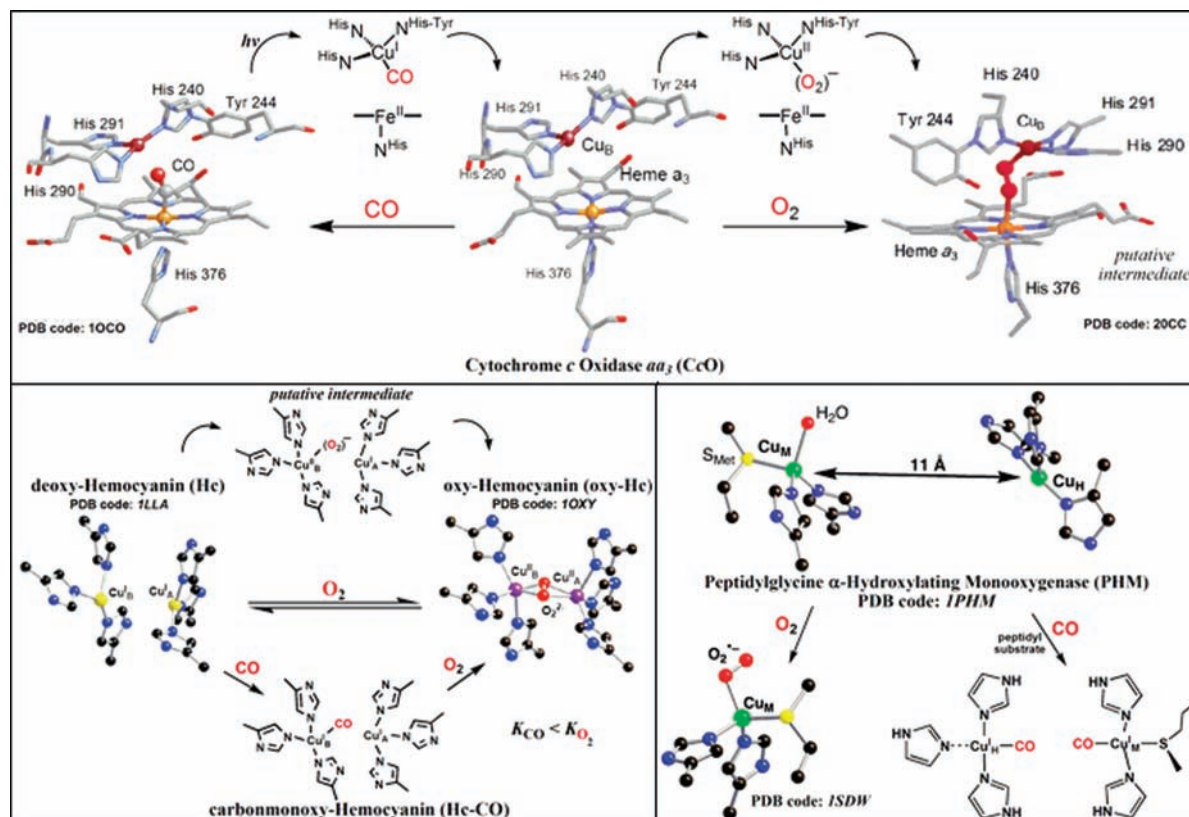


**Figure 1.** Overview of reduced copper containing protein active site  $O_2$  and CO interactions, highlighting the heme $a_3$ –Cu $B$  active site for  $O_2$  binding/reduction of mitochondrial cytochrome *c* oxidase (CcO), the arthropodal and molluscan hemolymph  $O_2$  carrier Hc, and the mammalian neuropeptide hormone-producing monooxygenase PHM.

as (ligand)Cu $^{II}$ – $O_2^{*}$ , is relatively rare.<sup>7–15</sup> Indeed, such species are implicated as key active-site entities in the (bio)chemistry of dioxygen activating copper enzymes.<sup>16–19</sup>

Time-resolved laser flash spectroscopy has been widely used to investigate small-molecule interactions with natural and

synthetic hemes.<sup>20–36</sup> By taking advantage of the extremely short time scale resolution of such photolytic methods, detailed mechanistic information has been achieved. For example, a wealth of knowledge has been gained about both hemoglobin and myoglobin by monitoring photoinitiated CO dissociation from heme–CO in the presence of  $O_2$ .<sup>37</sup> Also, in the heme–copper protein cytochrome *c* oxidase (CcO, Figure 1),

- (7) Woertink, J. S.; Smeets, P. J.; Groothaert, M. H.; Vance, M. A.; Sels, B. F.; Schoonheydt, R. A.; Solomon, E. I. *Proc. Natl. Acad. Sci. U.S.A.* **2009**, *106*, 18908–18913.
- (8) Zhang, C. X.; Kaderli, S.; Costas, M.; Kim, E.; Neuhold, Y. M.; Karlin, K. D.; Zuberbühler, A. D. *Inorg. Chem.* **2003**, *42*, 1807–1824.
- (9) Himes, R. A.; Karlin, K. D. *Curr. Opin. Chem. Biol.* **2009**, *13*, 119–131.
- (10) Maiti, D.; Lee, D. H.; Gaoutchenova, K.; Wurtele, C.; Holthausen, M. C.; Sarjeant, A. A. N.; Sundermeyer, J.; Schindler, S.; Karlin, K. D. *Angew. Chem., Int. Ed.* **2008**, *47*, 82–85.
- (11) Würtele, C.; Gaoutchenova, E.; Harms, K.; Holthausen, M. C.; Sundermeyer, J.; Schindler, S. *Angew. Chem., Int. Ed.* **2006**, *45*, 3867–3869.
- (12) Fujisawa, K.; Tanaka, M.; Morooka, Y.; Kitajima, N. *J. Am. Chem. Soc.* **1994**, *116*, 12079–12080.
- (13) Aboeella, N. W.; Kryatov, S. V.; Gherman, B. F.; Brennessel, W. W.; Young, V. G.; Sarangi, R.; Rybak-Akimova, E. V.; Hodgson, K. O.; Hedman, B.; Solomon, E. I.; Cramer, C. J.; Tolman, W. B. *J. Am. Chem. Soc.* **2004**, *126*, 16896–16911. For comparison,  $k_{O_2} \approx 10^4 \text{ M}^{-1} \text{ s}^{-1}$  for  $\beta\text{DkCu}^I$ .
- (14) Weitzer, M.; Schindler, S.; Brehm, G.; Schneider, S.; Hormann, E.; Jung, B.; Kaderli, S.; Zuberbühler, A. D. *Inorg. Chem.* **2003**, *42*, 1800–1806.
- (15) Fry, H. C.; Scaltrito, D. V.; Karlin, K. D.; Meyer, G. J. *J. Am. Chem. Soc.* **2003**, *125*, 11866–11871.
- (16) Itoh, S.; Fukuzumi, S. *Acc. Chem. Res.* **2007**, *40*, 592–600.
- (17) Itoh, S. *Curr. Opin. Chem. Biol.* **2006**, *10*, 115–122.
- (18) Prügge, S. T.; Eipper, B. A.; Mains, R. E.; Amzel, L. M. *Science* **2004**, *304*, 864–867.
- (19) Humphreys, K. J.; Mirica, L. M.; Wang, Y.; Klinman, J. P. *J. Am. Chem. Soc.* **2009**, *131*, 4657–4663.

- (20) Kitagawa, T.; Ogura, T. *Prog. Inorg. Chem.* **1997**, *45*, 431–479.
- (21) Larsen, R. W.; Mikšovská, J. *Coord. Chem. Rev.* **2007**, *251*, 1101–1127.
- (22) Fry, H. C.; Cohen, A. D.; Toscano, J. P.; Meyer, G. J.; Karlin, K. D. *J. Am. Chem. Soc.* **2005**, *127*, 6225–6230.
- (23) Fry, H. C.; Hoertz, P. G.; Wasser, I. M.; Karlin, K. D.; Meyer, G. J. *J. Am. Chem. Soc.* **2004**, *126*, 16712–16713.
- (24) Fry, H. C.; Lucas, H. R.; Zakharov, L. N.; Rheingold, A. L.; Meyer, G. J.; Karlin, K. D. *Inorg. Chim. Acta* **2008**, *361*, 1100–1115.
- (25) Lucas, H. R.; Meyer, G. J.; Karlin, K. D. *J. Am. Chem. Soc.* **2009**, *131*, 13924–13925.
- (26) Vos, M. H. *Biochim. Biophys. Acta* **2008**, *1777*, 15–31.
- (27) Dyer, R. B.; Peterson, K. A.; Stoutland, P. O.; Woodruff, W. H. *J. Am. Chem. Soc.* **1991**, *113*, 6276–6277.
- (28) Spiro, T. G.; Wasbotten, I. H. *J. Inorg. Biochem.* **2005**, *99*, 34–44.
- (29) Rousseau, D. L.; Han, S. *Methods Enzymol* **2002**, *354*, 351–368.
- (30) Ionascu, D.; Gruia, F.; Ye, X.; Yu, A. C.; Rosca, F.; Beck, C.; Demidov, A.; Olson, J. S.; Champion, P. M. *J. Am. Chem. Soc.* **2005**, *127*, 16921–16934.
- (31) Kapetanaki, S. M.; Field, S. J.; Hughes, R. J. L.; Watmough, N. J.; Liebl, U.; Vos, M. H. *Biochim. Biophys. Acta* **2008**, *1777*, 919–924.
- (32) Gibson, Q. H.; Greenwood, C. *Biochem. J.* **1963**, *86*, 541.
- (33) Greenwood, C.; Gibson, Q. H. *J. Biol. Chem.* **1967**, *242*, 1782.
- (34) Einarsdottir, O.; Szundi, I. *Biochim. Biophys. Acta* **2004**, *1655*, 263–273.
- (35) Szundi, I.; Rose, M. J.; Sen, I.; Eroy-Reveles, A. A.; Mascharak, P. K.; Einarsdottir, O. *Photochem. Photobiol.* **2006**, *82*, 1377–1384.
- (36) Soldatova, A. V.; Ibrahim, M.; Olson, J. S.; Czernuszewicz, R. S.; Spiro, T. G. *J. Am. Chem. Soc.* **2010**, *132*, 4614–4625.

the characterization of photodriven CO transfer (as a surrogate for O<sub>2</sub> and potentially NO<sup>38</sup>) from heme<sub>a3</sub>–CO to Cu<sub>B</sub> suggested that the Cu<sub>B</sub> site was a “doorway” for small molecules into and out of the heterobimetallic active site.<sup>3,27</sup> Assuming a common O<sub>2</sub> mechanistic pathway and with some indirect evidence existing,<sup>39–41</sup> a Cu<sup>II</sup><sub>B</sub>–O<sub>2</sub><sup>•–</sup> intermediate is assumed to precede any heme<sub>a3</sub>/O<sub>2</sub> interactions; a putative peroxo-bridged CcO intermediate that was crystallized is shown in Figure 1.

A key aspect for accomplishing such photoinitiated processes is the high binding affinity of heme systems for CO ( $K_{CO} > K_{O_2}$ ), as exploited by the “flash-and-trap” experiment pioneered by Gibson and co-workers.<sup>32,33</sup> Similar studies involving CO and O<sub>2</sub> have not been accomplished for the well-characterized type-3 binuclear copper proteins hemocyanin (Hc; Figure 1), tyrosinase (Tyr; widespread monooxygenase, converting phenols to *o*-catechols and *o*-quinones), and catechol oxidase (*o*-catechol → *o*-quinone), mainly due to the opposite behavior, a high stability ( $K_{O_2} > K_{CO}$ ) of their 2:1 copper–dioxygen adduct, a dicopper(II)– $\mu$ - $\eta^2$ : $\eta^2$ -(*side-on*)-peroxo protein species.<sup>3,16,42,43</sup>

Early work established that only one small molecule, CO or O<sub>2</sub>, binds per dicopper active site, presumably to Cu<sub>B</sub>, and that the close proximity of the two copper centers (Cu<sub>A</sub> and Cu<sub>B</sub>) enables fast electron transfer (ET) for the two-electron reduction of O<sub>2</sub>.<sup>3,16,42,43</sup> However, even following photoexcitation and subsequent dissociation of O<sub>2</sub> from oxy-Tyr<sup>44</sup> and/or oxy-Hc,<sup>45,46</sup> a Cu<sup>II</sup><sub>B</sub>–O<sub>2</sub><sup>•–</sup> adduct has not been detected and instead only implicated through theoretical modeling.<sup>16,47</sup> Nevertheless, Hirota, Bubacco, and co-workers recently used flash photolysis and complementary K-edge X-ray absorption spectroscopy (XAS) measurements to show that the O<sub>2</sub> binding rate constant ( $k_{O_2}$ ) for a deoxy-Hc was dependent on the copper(I) coordination geometry.<sup>45</sup> In addition, the thermodynamic data ( $\Delta H^\ddagger$ ,  $\Delta S^\ddagger$ ) they obtained were comparable to those reported for mononuclear synthetic model compounds, which emphasizes the important relationship between synthetic bioinorganic chemistry and metallobiochemistry.

In peptidylglycine  $\alpha$ -hydroxylating monooxygenase (PHM), the active site contains two uncoupled copper centers (Cu<sup>•••</sup>Cu, ~11 Å; Cu<sub>A</sub>  $\equiv$  Cu<sub>H</sub>, Cu<sub>B</sub>  $\equiv$  Cu<sub>M</sub>). A copper(II)–superoxo species, which is suggested by some to be the key intermediate that initiates substrate oxidation reactions, has been characterized by X-ray crystallography.<sup>18</sup> This “end-on”  $\eta^1$ -bound (to Cu<sub>M</sub>) “pre-catalytic” copper–dioxygen adduct is shown in Figure 1. Interestingly, CO binds the catalytic (Cu<sub>M</sub>) site as well as to

the ET center (Cu<sub>H</sub>), the latter only if substrate is present.<sup>48,49</sup> Key Cu<sup>I</sup>/O<sub>2</sub> 1:1 species are also implicated in the enzymatic reactions carried out by copper amine oxidase (CAO)<sup>50–52</sup> and galactose oxidase.<sup>19</sup>

As mentioned, CO–heme protein active site interactions have been widely investigated. Similarly, the use of CO for investigation of copper proteins has provided tremendous insight and fundamental information.<sup>3</sup> The occurrence of detectable and significant variations in active-site copper ligation within a given protein has been noted and is also present in proteins from different species or organisms. The  $\nu_{CO}$  values of carbon-monoxo–copper proteins are highly variable, even when equally coordinated by three imidazolyl N-donors. For example,  $\nu_{CO}$  values corresponding to the Cu<sup>I</sup>–CO adducts of CAO (2061–2085 cm<sup>–1</sup>),<sup>53</sup> the Cu<sub>H</sub>–CO site of PHM (2062 cm<sup>–1</sup>),<sup>48</sup> and the Cu<sub>B</sub>–CO sites of CcO (2053–2063 cm<sup>–1</sup>),<sup>54–56</sup> nitrite reductase (NiR; 2050 cm<sup>–1</sup>),<sup>57</sup> and Hc–CO (2043–2063 cm<sup>–1</sup>)<sup>58</sup> exhibit large differences. Such variations in  $\nu_{CO}$  for N<sub>3</sub>Cu<sup>I</sup>–CO adducts indicate subtle changes in the local active-site environment (e.g., coordination geometry changes, dielectric of the medium, etc.) alter the copper ion’s electron density and thus back-donation to the ligated carbon monoxide. This likely relates to or explains the diverse O<sub>2</sub> and/or NO reactivity among various copper proteins.

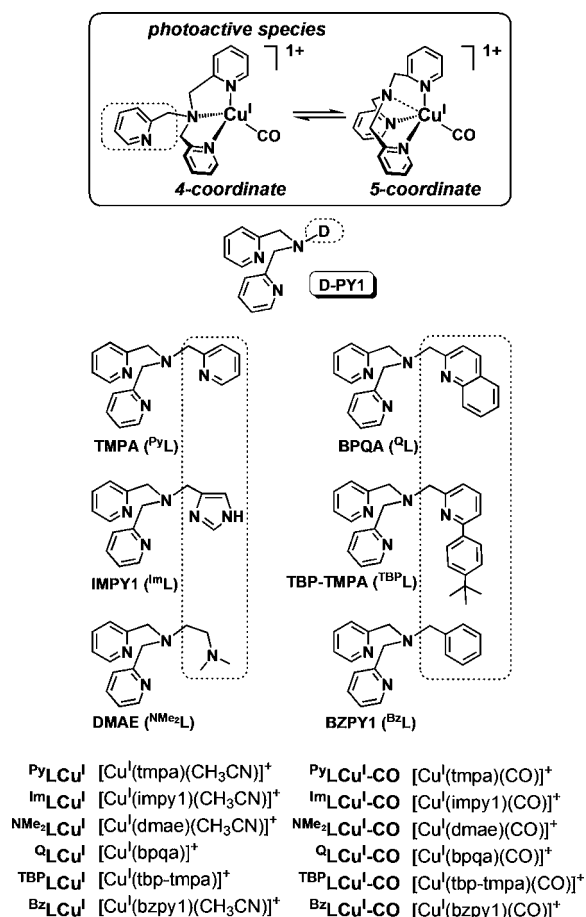
With this background, one of our goals is to develop an understanding of the kinetics and thermodynamics of copper(I)-mediated small-molecule interactions, specifically in this report with CO and O<sub>2</sub>. Carbon monoxide is a good surrogate for dioxygen, even while possessing redox-inactive binding characteristics. In addition, copper(I)–carbonyl adducts are typically more stable than their 1:1 copper–dioxygen counterparts and therefore easier to study. By gaining a deeper understanding of how the detailed nature of the ligand environment affects CO binding to copper(I), as has been carried out in natural systems, reliable comparisons can be made to Cu<sup>I</sup>/O<sub>2</sub> and potentially NO (bio)chemistries.

We previously reported on the CO photodissociation chemistry of a number of cuprous pyridylalkylamine compounds.<sup>59</sup> Effects upon systematic variations in the ligand framework were examined (i) via changes in the electron-donating ability of TMPA {<sup>Py</sup>L = tris(2-pyridylmethyl)amine} through addition of 4-pyridyl substituents (R-<sup>Py</sup>L; R = N(CH<sub>3</sub>)<sub>2</sub>, CH<sub>3</sub>O); (ii) by an increase in the chelate ring-size from 5-membered to 6-membered ligand coordination

- (37) Birukou, I.; Schweers, R. L.; Olson, J. S. *J. Biol. Chem.* **2010**, *285*, 8840–8854.  
 (38) Ohta, K.; Muramoto, K.; Shinzawa-Itoh, K.; Yamashita, E.; Yoshikawa, S.; Tsukihara, T. *Acta Crystallogr. F* **2010**, *66*, 251–253.  
 (39) Babcock, G. T.; Floris, R.; Nilsson, T.; Pressler, M.; Varotsis, C.; Vollenbroek, E. *Inorg. Chim. Acta* **1996**, *243*, 345–353.  
 (40) Oliveberg, M.; Malmstrom, B. G. *Biochemistry* **1992**, *31*, 3560–3563.  
 (41) Muramoto, K.; Ohta, K.; Shinzawa-Itoh, K.; Kanda, K.; Taniguchi, M.; Nabekura, H.; Yamashita, E.; Tsukihara, T.; Yoshikawa, S. *Proc. Natl. Acad. Sci. U.S.A.* **2010**, *107*, 7740–7745.  
 (42) Magnus, K. A.; Hazes, B.; Tonthat, H.; Bonaventura, C.; Bonaventura, J.; Hol, W. G. J. *Proteins* **1994**, *19*, 302–309.  
 (43) Solomon, E. I.; Tuzcek, F.; Root, D. E.; Brown, C. A. *Chem. Rev.* **1994**, *94*, 827–856.  
 (44) Hirota, S.; Kawahara, T.; Lonardi, E.; de Waal, E.; Funasaki, N.; Canters, G. W. *J. Am. Chem. Soc.* **2005**, *127*, 17966–17967.  
 (45) Hirota, S.; Kawahara, T.; Beltrami, M.; Di Muro, P.; Magliozzo, R. S.; Peisach, J.; Powers, L. S.; Tanaka, N.; Nagao, S.; Bubacco, L. *J. Biol. Chem.* **2008**, *283*, 31941–31948.  
 (46) Floyd, J. S.; Haralampus-Grynawski, N.; Ye, T.; Zheng, B.; Simon, J. D.; Edington, M. D. *J. Phys. Chem. B* **2001**, *105*, 1478–1483.  
 (47) Guëll, M.; Siegbahn, P. E. M. *J. Biol. Inorg. Chem.* **2007**, *12*, 1251–1264.

- (48) Jaron, S.; Blackburn, N. J. *Biochemistry* **1999**, *38*, 15086–15096.  
 (49) Jaron, S.; Mains, R. E.; Eipper, B. A.; Blackburn, N. J. *Biochemistry* **2002**, *41*, 13274–13282.  
 (50) Wilmot, C. M.; Hajdu, J.; McPherson, M. J.; Knowles, P. F.; Phillips, S. E. V. *Science* **1999**, *286*, 1724–1728.  
 (51) Mukherjee, A.; Smirnov, V. V.; Lanci, M. P.; Brown, D. E.; Shepard, E. M.; Dooley, D. M.; Roth, J. P. *J. Am. Chem. Soc.* **2008**, *130*, 9459–9473.  
 (52) Shepard, E. M.; Okonski, K. M.; Dooley, D. M. *Biochemistry* **2008**, *47*, 13907–13920.  
 (53) Hirota, S.; Iwamoto, T.; Tanizawa, K.; Adachi, O.; Yamauchi, O. *Biochemistry* **1999**, *38*, 14256–14263.  
 (54) Alben, J. O.; Moh, P. P.; Fiamingo, F. G.; Altschuld, R. A. *Proc. Natl. Acad. Sci. U.S.A.* **1981**, *78*, 234–237.  
 (55) Hill, J.; Goswitz, V. C.; Calhoun, M.; Garciahorsman, J. A.; Lemieux, L.; Alben, J. O.; Gennis, R. B. *Biochemistry* **1992**, *31*, 11435–11440.  
 (56) Einarsdottir, O.; Killough, P. M.; Fee, J. A.; Woodruff, W. H. *J. Biol. Chem.* **1989**, *264*, 2405–2408.  
 (57) Zhang, H. M.; Boulanger, M. J.; Mauk, A. G.; Murphy, M. E. P. *J. Phys. Chem. B* **2000**, *104*, 10738–10742.  
 (58) Fager, L. Y.; Alben, J. O. *Biochemistry* **1972**, *11*, 4786–4792.  
 (59) Fry, H. C.; Lucas, H. R.; Sarjeant, A. A. N.; Karlin, K. D.; Meyer, G. J. *Inorg. Chem.* **2008**, *47*, 241–256.

Chart 1



to copper as in bis[(3-pyridyl)methyl]-2-(2-pyridyl)ethylamine (PMEA) vs bis[2-(2-pyridyl)ethyl]-(2-pyridyl)methylamine (PMAP); and (iii) with a change in the donor group moieties as in bis(2-quinolylmethyl)(2-pyridylmethyl)amine (BQPA). The effort advanced our understanding of the coordination environment required for ligand–copper(I)–carbonyl photodissociation and rebinding of carbon monoxide; tridentate coordination from the tetradentate ligand moieties to the copper(I)–carbonyl center (overall four-coordinate) was required (Chart 1), in which one N-donor moiety was “dangling”, i.e., uncoordinated. Observed variations in kinetics and thermodynamics were shown to derive from particular changes in the copper complex electron-releasing properties, coordination geometry, and/or steric effects.

The subject and direction of the work discussed herein examines the effect of changes in the dangling N-donor moiety within various ligand–copper(I) complexes (P'LCu<sup>I</sup>) on both 1:1 CO and O<sub>2</sub> binding kinetics and thermodynamics as well as CO and O<sub>2</sub> coordination dynamics. Variable-temperature transient absorbance (TA) laser flash photolysis in tetrahydrofuran (THF) solvent has been employed. The P'L ligand series consists of potentially tetradentate ligands with the same PY1 [L, bis(2-pyridylmethyl)amine] core, but with variable N-donor moieties (D); see Chart 1. For the studies of CO binding, a tridentate ligand species Bz'L was also examined as a “standard” for comparison.<sup>25</sup> As will be described, drastic differences in

Cu<sup>I</sup>–CO and Cu<sup>I</sup>–O<sub>2</sub> chemistry result from seemingly minor changes in the P'LCu<sup>I</sup> ligand framework.

## Experimental Section

See Supporting Information for details concerning materials and methods, references to syntheses of previously published ligands, and complexes along with synthetic procedures for new compounds.

## Results

**Synthesis of Ligand–Copper(I) (P'LCu<sup>I</sup>) and Ligand–Copper(I)–Carbonyl (P'LCu<sup>I</sup>–CO) Complexes.** The ligands (P'L) used in the present study were previously reported and characterized in detail (Chart 1).<sup>60–65</sup> The ligand–copper(I) complexes as B(C<sub>6</sub>F<sub>5</sub>)<sub>4</sub><sup>−</sup> salts (P'LCu<sup>I</sup>) were straightforwardly prepared by addition of [Cu'(MeCN)<sub>4</sub>]B(C<sub>6</sub>F<sub>5</sub>)<sub>4</sub> to the appropriate ligand in deoxygenated Et<sub>2</sub>O and isolated by slow precipitation in dry, air-free pentane under an argon atmosphere.<sup>8,60,64–66</sup> The B(C<sub>6</sub>F<sub>5</sub>)<sub>4</sub><sup>−</sup> counteranion was chosen to afford greater solubility in THF solvent.

The presence of coordinated acetonitrile (CH<sub>3</sub>CN) in the isolated copper(I) complexes of Py'LCu<sup>I</sup>, Im'LCu<sup>I</sup>, NMe<sub>2</sub>LCu<sup>I</sup>, and Bz'LCu<sup>I</sup> was confirmed through elemental (C, H, N) combustion analysis and <sup>1</sup>H NMR spectroscopy studies in deuterated nitromethane (CD<sub>3</sub>NO<sub>2</sub>).<sup>8,60,64,65</sup> The X-ray crystal structures of Bz'LCu<sup>I</sup> and the ClO<sub>4</sub><sup>−</sup> salts of NMe<sub>2</sub>LCu<sup>I</sup> and Py'LCu<sup>I</sup> were previously reported, with each containing an exogenously derived CH<sub>3</sub>CN molecule.<sup>60,62,67</sup> As expected for a tridentate ligand system, Bz'LCu<sup>I</sup> binds CH<sub>3</sub>CN the strongest, as supported by the shorter Cu–N<sub>nitrile</sub> bond distance of 1.900(4) Å versus 2.038(2) Å for NMe<sub>2</sub>LCu<sup>I</sup> and 1.990(12) Å for Py'LCu<sup>I</sup>, which are complexes with tetradentate N<sub>4</sub> ligation. Acetonitrile does not coordinate to TBP'LCu<sup>I</sup> and Q'LCu<sup>I</sup> based on the characterization methods described above and X-ray structural characterization, *vide infra*.

Ligand–copper(I)–carbonyl complexes (P'LCu<sup>I</sup>–CO) were formed *in situ* through vigorous CO bubbling into dry THF solutions. TBP'LCu<sup>I</sup>–CO and Bz'LCu<sup>I</sup>–CO were isolated as overall four-coordinate species, i.e., possessing a dangling ligand donor arm (*vide infra*), following dissolution of TBP'LCu<sup>I</sup> and Bz'LCu<sup>I</sup> in CO-saturated Et<sub>2</sub>O and layering with pentane for slow diffusion.<sup>68</sup> In a previous study, Py'LCu<sup>I</sup>–CO was isolated as a five-coordinate species, i.e., with all ligand N donors coordinated.<sup>59</sup>

**X-ray Crystallography of TBP'LCu<sup>I</sup>–CO, Bz'LCu<sup>I</sup>–CO, Q'LCu<sup>I</sup>.** ORTEP diagrams of TBP'LCu<sup>I</sup>–CO (A) and Bz'LCu<sup>I</sup>–CO (B) are shown in Figure 2, and that for Q'LCu<sup>I</sup> is given in Figure 3; selected bond lengths and angles are provided in the figure captions.<sup>68</sup> Both ligand–copper(I)–carbonyl structures display

(60) Lucas, H. R.; Li, L.; Sarjeant, A. A. N.; Vance, M. A.; Solomon, E. I.; Karlin, K. D. *J. Am. Chem. Soc.* **2009**, *131*, 3230–3245.

(61) Tyeklár, Z.; Jacobson, R. R.; Wei, N.; Murthy, N. N.; Zubieta, J.; Karlin, K. D. *J. Am. Chem. Soc.* **1993**, *115*, 2677–2689.

(62) Weitzer, M.; Schatz, M.; Hampel, F.; Heinemann, F. W.; Schindler, S. *J. Chem. Soc., Dalton Trans.* **2002**, 686–694.

(63) Wei, N.; Murthy, N. N.; Chen, Q.; Zubieta, J.; Karlin, K. D. *Inorg. Chem.* **1994**, *33*, 1953–1965.

(64) Maiti, D.; Lucas, H. R.; Sarjeant, A. A. N.; Karlin, K. D. *J. Am. Chem. Soc.* **2007**, *129*, 6998–6999.

(65) Lee, Y.; Park, G. Y.; Lucas, H. R.; Vajda, P. L.; Kamaraj, K.; Vance, M. A.; Milligan, A. E.; Woertink, J. S.; Siegler, M. A.; Sarjeant, A. A. N.; Zakharov, L. N.; Rheingold, A. L.; Solomon, E. I.; Karlin, K. D. *Inorg. Chem.* **2009**, *48*, 11297–11309.

(66) Liang, H. C.; Kim, E.; Incarvito, C. D.; Rheingold, A. L.; Karlin, K. D. *Inorg. Chem.* **2002**, *41*, 2209–2212.

(67) Lim, B. S.; Holm, R. H. *Inorg. Chem.* **1998**, *37*, 4898–4908.

(68) See Supporting Information.

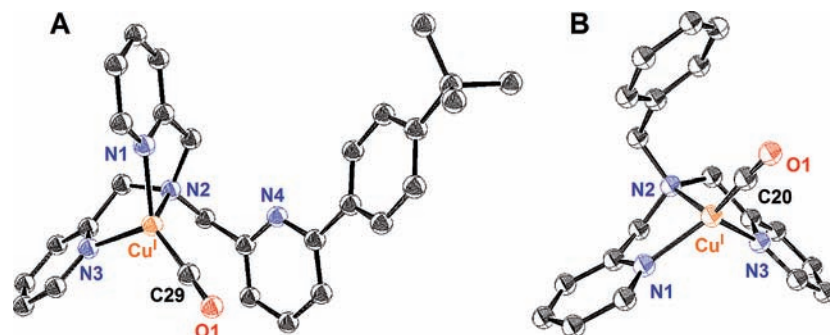


**Figure 2.** ORTEP diagrams of (A)  $\text{TBPLCu}^{\text{I}}\text{-CO}$  and (B)  $\text{BzLCu}^{\text{I}}\text{-CO}$ ; hydrogen atoms and the  $\text{B}(\text{C}_6\text{F}_5)_4$  counteranion have been omitted for clarity. Selected bond lengths: (A) Cu–C 1.801(6) Å, C–O 1.124(6) Å, Cu–N<sub>alkylamine</sub> 2.147(4) Å, Cu–N<sub>pyridine(aveg)</sub> 2.051(5) Å; and (B) Cu–C 1.815(1) Å, C–O 1.123(2) Å, Cu–N<sub>alkylamine</sub> 2.158(6) Å, and Cu–N<sub>pyridine(aveg)</sub> 2.048(3) Å. Selected bond angles: (A) C–Cu–N<sub>pyridine(aveg)</sub> 121.4(2)°, C–Cu–N<sub>alkylamine</sub> 131.0(0)°, N<sub>pyridine(aveg)</sub>–Cu–N<sub>alkylamine</sub> 81.0(9)°, N<sub>pyridyl</sub>–Cu–N<sub>pyridyl</sub> 109.6(0)°; and (B) C–Cu–N<sub>pyridine(aveg)</sub> 121.95(7)°, C–Cu–N<sub>alkylamine</sub> 129.94(7)°, N<sub>pyridine(aveg)</sub>–Cu–N<sub>alkylamine</sub> 80.80(6)°, and N<sub>pyridyl</sub>–Cu–N<sub>pyridyl</sub> 108.94(6)°.<sup>68</sup>

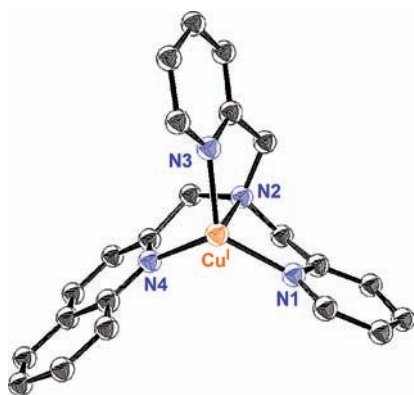


**Figure 3.** ORTEP diagram of  $\text{QLCu}^{\text{I}}$  with hydrogen atoms and the  $\text{B}(\text{C}_6\text{F}_5)_4$  counteranion omitted for clarity. Selected bond lengths: Cu–N<sub>pyridine(1)</sub> 1.988(2) Å, Cu–N<sub>pyridine(3)</sub> 2.006(2) Å, Cu–N<sub>alkylamine(2)</sub> 2.185(2) Å, and Cu–N<sub>quinoline(4)</sub> 2.012(2) Å. Selected bond angles N<sub>pyridyl(aveg)</sub>–Cu–N<sub>alkylamine(2)</sub> 82.84(8)°, N<sub>pyridyl(1)</sub>–Cu–N<sub>pyridyl(3)</sub> 123.63(8)°, N<sub>pyridyl(1)</sub>–Cu–N<sub>quinolyl(4)</sub> 119.95(8)°, N<sub>amine(2)</sub>–Cu–N<sub>quinolyl(4)</sub> 82.58(7)°, and N<sub>pyridyl(3)</sub>–Cu–N<sub>quinolyl(4)</sub> 111.70(8)°.<sup>68</sup>

an overall four-coordinate geometry consisting of the copper(I) ion coordinated by the apical alkylamino nitrogen, two pyridyl donors, and the carbon from a coordinated CO molecule. The N<sub>pyridyl</sub>–Cu–N<sub>amine</sub> angles of  $\sim 81^\circ$  are rather severe in comparison to other structurally characterized four-coordinate copper(I) carbonyl complexes, which have average N–Cu–N bond angles of  $\sim 95^\circ$ .<sup>59,69–75</sup> The Cu–C bond length is shorter (stronger) for  $\text{TBPLCu}^{\text{I}}\text{-CO}$  (1.801 Å) in comparison to that observed for  $\text{BzLCu}^{\text{I}}\text{-CO}$  (1.815 Å), possibly due to an indirect increase in overall electron density in the former complex, with the difference being a *tert*-butylphenyl (tbp)-substituted pyridine vs a benzyl substituent on the **L** tridentate moiety; see Chart 1.

A tridentate (N<sub>3</sub>) coordination mode for  $\text{TBPLCu}^{\text{I}}\text{-CO}$  is of interest due to the tetradentate (N<sub>4</sub>) nature of **TBPL**; the 6-tbp-substituted pyridyl arm dissociates, i.e., is dangling, due to the increased steric constraints. However, in the absence of CO, all three pyridyl donors as well as the bridgehead alkylamine coordinate to the copper(I) ion, as supported by the known X-ray crystal structure of  $\text{TBPLCu}^{\text{I}}$ .<sup>64</sup> The coordination sphere of  $\text{TBPLCu}^{\text{I}}$  did not include a coordinated acetonitrile molecule as is generally observed for analogous ligand–copper(I) complexes, *vide supra*.

Similar structural characteristics have been reported on the basis of X-ray crystallographic analysis of the copper(I) complex and copper(I)–carbonyl adduct of BQPA.<sup>59,63,76</sup> For  $[\text{Cu}^{\text{I}}(\text{bqpa})]\text{B}(\text{C}_6\text{F}_5)_4$ , all four N-donor moieties coordinate to the copper(I) ion and one quinolyl donor arm dissociates upon coordination of CO or triphenylphosphine (PPh<sub>3</sub>).<sup>63</sup> As shown in Figure 3, the X-ray crystal structure of  $\text{QLCu}^{\text{I}}$  is four-coordinate, with both pyridyl donors, the quinolyl donor, and the bridgehead alkylamine coordinated to the cuprous center. An X-ray crystal structure of  $\text{QLCu}^{\text{I}}\text{-CO}$  has not been obtained, but IR spectroscopic data support a tridentate ligand coordination in which the quinolyl arm is dangling, *vide infra*.

**Infrared Spectroscopy ( $\nu_{\text{CO}}$ : Solution and Solid State).** The solution (THF) and solid-state (Nujol mull)  $\nu_{\text{CO}}$  values of the ligand–copper(I)–carbonyl complexes ( $\text{PLCu}^{\text{I}}\text{-CO}$ ) were determined in order to gauge the ligand–N-donor ability of the variable D-moiety as well as to elucidate potential differences in coordination number and/or the overall geometry. As described above, in part, the CO stretching frequencies ( $\nu_{\text{CO}}$ ) of synthetic copper(I)–carbonyl complexes and carbonmonoxy–copper proteins are found to be in the range  $\nu_{\text{CO}} = 2035\text{--}2137\text{ cm}^{-1}$ .<sup>3,73,77–82</sup> Notably, the characteristic  $\nu_{\text{CO}}$  values of copper(I)–carbonyl proteins coordinated by three imidazolyl N-donors are usually  $\Delta\nu_{\text{CO}} = 20\text{--}40\text{ cm}^{-1}$  lower than those of synthetic species with three N-donors.<sup>3,79</sup> This suggests that

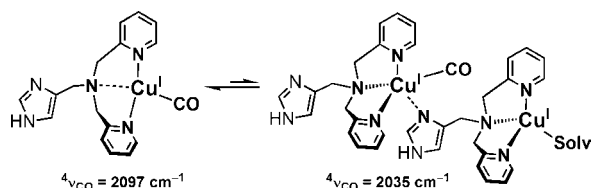
- (69) Pasquali, M.; Marini, G.; Floriani, C.; Gaetanimanfredotti, A.; Guastini, C. *Inorg. Chem.* **1980**, *19*, 2525–2531.  
 (70) Kitajima, N.; Fujisawa, K.; Fujimoto, C.; Morooka, Y.; Hashimoto, S.; Kitagawa, T.; Toriumi, K.; Tatsumi, K.; Nakamura, A. *J. Am. Chem. Soc.* **1992**, *114*, 1277–1291.  
 (71) Karlin, K. D.; Tyeklar, Z.; Farooq, A.; Haka, M. S.; Ghosh, P.; Cruse, R. W.; Gultneh, Y.; Hayes, J. C.; Toscano, P. J.; Zubieta, J. *Inorg. Chem.* **1992**, *31*, 1436–1451.  
 (72) Ardizzoia, G. A.; Beccalli, E. M.; Lamonica, G.; Masciocchi, N.; Moret, M. *Inorg. Chem.* **1992**, *31*, 2706–2711.  
 (73) Imai, S.; Fujisawa, K.; Kobayashi, T.; Shirasawa, N.; Fujii, H.; Yoshimura, T.; Kitajima, N.; Moro-oka, Y. *Inorg. Chem.* **1998**, *37*, 3066–3070.  
 (74) Conry, R. R.; Ji, G. Z.; Tipton, A. A. *Inorg. Chem.* **1999**, *38*, 906–913.  
 (75) Reger, D. L.; Collins, J. E. *Organometallics* **1996**, *15*, 2029–2032.

- (76) Unpublished work.  
 (77) Himes, R. A.; Park, G. Y.; Barry, A. N.; Blackburn, N. J.; Karlin, K. D. *J. Am. Chem. Soc.* **2007**, *129*, 5352–5353.  
 (78) Pasquali, M.; Floriani, C. *Copper(I)–Carbon Monoxide Chemistry: Recent Advances and Perspectives*, In *Copper Coordination Chemistry: Biochemical & Inorganic Perspectives*; Karlin, K. D. Zubieta, J., Eds.; Adenine Press: New York, 1983; pp 311–330.  
 (79) Rondelez, Y.; Seneque, O.; Rager, M. N.; Duprat, A. F.; Reinaud, O. *Chem.–Eur. J.* **2000**, *6*, 4218–4226.  
 (80) Jonas, R. T.; Stack, T. D. P. *Inorg. Chem.* **1998**, *37*, 6615–6629.  
 (81) Fujisawa, K.; Ono, T.; Ishikawa, Y.; Amir, N.; Miyashita, Y.; Okamoto, K.; Lehnert, N. *Inorg. Chem.* **2006**, *45*, 1698–1713.  
 (82) Dias, H. V. R.; Lu, H. L. *Inorg. Chem.* **1995**, *34*, 5380.

**Table 1.** Carbonyl Stretching Frequencies for  $^{\text{D}}\text{LCu}^{\text{I}}\text{-CO}$  Complexes and Cyclic Voltammetry Data for  $^{\text{D}}\text{LCu}^{\text{I}}$  Complexes

compound	neat solid	THF solution	$E_{1/2}^b$	$\Delta E^b$
$^{\text{Im}}\text{LCu}^{\text{I}}\text{-CO}$	2097, 2035(sm)	2087, 2063	-445	110
$^{\text{NMe}_2}\text{LCu}^{\text{I}}\text{-CO}$	2097	2090	-445	85
$^{\text{Py}}\text{LCu}^{\text{I}}\text{-CO}$	2077	2091, 2074(sh)	-410	75
$^{\text{Q}}\text{LCu}^{\text{I}}\text{-CO}$	2090	2091	-325	110
$^{\text{TBP}}\text{LCu}^{\text{I}}\text{-CO}$	2091	2092	-325	115
$^{\text{Bz}}\text{LCu}^{\text{I}}\text{-CO}$	2093	2093	-225	155

<sup>a</sup> Abbreviations: sm = small, sh = shoulder. <sup>b</sup> Electrochemical measurements are of copper(I) complexes (not carbonyl) in deoxygenated  $\text{CH}_3\text{CN}$ . Potentials are reported versus the  $\text{Fc}^+/\text{Fc}$  redox couple and are rounded to the nearest 5 mV.

**Chart 2**

copper–protein imidazole groups are exceptionally strong donors, and relative to most synthetic copper(I)–carbonyl complexes, this leads to weaker C–O (but stronger Cu–C) bonds.

#### Solution-State IR Spectroscopic and Structural Properties.

As discussed in the Introduction (Chart 1), previous work established that an equilibrium mixture of four- ( $^4\nu_{\text{CO}} = 2090 \text{ cm}^{-1}$ ) and five-coordinate ( $^5\nu_{\text{CO}} = 2077 \text{ cm}^{-1}$ ) copper(I)–carbonyl isomers exist for  $^{\text{Py}}\text{LCu}^{\text{I}}\text{-CO}$  in THF solvent (Table 1 and Chart 1). Similarly, an equilibrium mixture of  $^{\text{Im}}\text{LCu}^{\text{I}}\text{-CO}$  isomers exists in THF,  $^4\nu_{\text{CO}} = 2087 \text{ cm}^{-1}$  and  $^5\nu_{\text{CO}} = 2063 \text{ cm}^{-1}$ . The lower-energy shift of  $\Delta^5\nu_{\text{CO}} = 14 \text{ cm}^{-1}$  for  $^{\text{Im}}\text{LCu}^{\text{I}}\text{-CO}$  isomer in comparison to  $^{\text{Py}}\text{LCu}^{\text{I}}\text{-CO}$  indicates that the imidazole in  $^{\text{Im}}\text{L}$  is a stronger donor for copper(I) than the pyridine in  $^{\text{Py}}\text{L}$ . However, the hard aliphatic amine group within  $^{\text{NMe}_2}\text{LCu}^{\text{I}}\text{-CO}$  does not ligate at all in THF solution, as indicated by the single CO stretch at  $2090 \text{ cm}^{-1}$ .

Consistent with their X-ray crystal structures,  $^{\text{TBP}}\text{LCu}^{\text{I}}\text{-CO}$  and  $^{\text{Bz}}\text{LCu}^{\text{I}}\text{-CO}$  are four-coordinate structures in THF solution with  $^4\nu_{\text{CO}}$  values of 2091 and  $2093 \text{ cm}^{-1}$ , respectively (see Table 1). THF solution data for  $^{\text{Q}}\text{LCu}^{\text{I}}\text{-CO}$  reveal the same  $\text{N}_3\text{Cu}^{\text{I}}\text{-CO}$  coordination based on the  $^4\nu_{\text{CO}}$  value. Overall, the CO stretching frequencies for all four-coordinate  $^{\text{D}}\text{LCu}^{\text{I}}\text{-CO}$  solution complexes are approximately equal,  $^4\nu_{\text{CO}}(\text{avg}) = 2091 \text{ cm}^{-1}$ , indicating that the dangling arm throughout the series must be the D-donor moiety, as depicted in Chart 1.

**Solid-State IR Spectroscopic and Structural Properties.** The  $^4\nu_{\text{CO}}$  values of the isolated  $^{\text{Im}}\text{LCu}^{\text{I}}\text{-CO}$  and  $^{\text{NMe}_2}\text{LCu}^{\text{I}}\text{-CO}$  species were both centered at  $2097 \text{ cm}^{-1}$  in Nujol mull spectra, suggesting that the imidazole or aliphatic dimethylamine donor moieties do not coordinate in the static solid-state structure. Since these values are higher than the solution-state  $^4\nu_{\text{CO}}$  values, the  $^{\text{D}}\text{L}$  ligation may be somewhat more two-coordinate in nature; i.e., perhaps the aliphatic amine nitrogen is less strongly bound than for the other cases (Chart 2). In the solid state,  $^{\text{Py}}\text{LCu}^{\text{I}}\text{-CO}$  has an overall five-coordinate structure.<sup>59</sup>

For  $^{\text{Im}}\text{LCu}^{\text{I}}\text{-CO}$ , an additional very low energy and intensity CO stretch at  $2035 \text{ cm}^{-1}$  is observed in the solid state. Such a low  $\nu_{\text{CO}}$  value suggests a coordination environment with anionic ligand donors, or three strong nonchelating N donors, as is known elsewhere.<sup>3,78</sup> In previous work, the electron-donating

ability of the four-coordinate R- $^{\text{Py}}\text{L}$  ligand series was increased by introduction of *para*-substituents such as  $\text{R} = \text{N}(\text{CH}_3)_2$  and  $\text{CH}_3\text{O}$  (Chart 2).<sup>59</sup> Here,  $\nu_{\text{CO}}$  values shifted to lower energy by  $14\text{--}28 \text{ cm}^{-1}$ , e.g.,  $\nu_{\text{CO}} = 2049 \text{ cm}^{-1}$  for  $[\text{Cu}^{\text{I}}(\text{NMe}_2\text{-}^{\text{Py}}\text{L})(\text{CO})]^+$  in THF. To explain the very low  $2035 \text{ cm}^{-1}$   $\nu_{\text{CO}}$  value, we suggest that the dangling imidazolyl moiety of  $^{\text{Im}}\text{LCu}^{\text{I}}\text{-CO}$  may coordinate to a different  $^{\text{Im}}\text{LCu}^{\text{I}}$  complex, forming a dimeric structure (see Chart 2). Pyridyl  $\pi\text{-}\pi$  stacking may facilitate formation of such a structure, as has been observed elsewhere for copper(I) structures.<sup>83–85</sup>

**Electrochemical Studies.** Copper(II/I) redox chemistry was examined through cyclic voltammetry measurements carried out on the ligand–copper(I) complexes ( $^{\text{D}}\text{LCu}^{\text{I}}$ ). Quasi-reversible single electron-transfer processes ( $i_{\text{pc}}/i_{\text{pa}} \approx 1$ ) with peak-to-peak separations between  $\Delta E = 75$  and  $155 \text{ mV}$  were observed (Table 1). The  $\text{Cu}^{\text{II}}/\text{Cu}^{\text{I}}$  redox potentials, i.e., electron transfer, are largely affected by structural alterations prompted by changes in oxidation states as well as steric hindrance induced by ligand variations. Overall, the trend of  $\text{Cu}^{\text{II/I}}$  half-wave potentials ( $E_{1/2}$ ) was similar to the trend of the  $^4\nu_{\text{CO}}$  values of  $^{\text{D}}\text{LCu}^{\text{I}}\text{-CO}$  species in THF (see Table 1). Ligand–copper complexes with more negative  $E_{1/2}$  values favor a higher oxidation state ( $\text{Cu}^{\text{II}}$ ) and suggest a more donating ligand system. For example, the formally tridentate  $^{\text{Bz}}\text{LCu}^{\text{I}}$  has the highest redox potential of  $-225 \text{ mV}$ , hence favoring a lower oxidation state.

The same  $E_{1/2}$  values were measured for  $^{\text{Q}}\text{LCu}^{\text{I}}$  and  $^{\text{TBP}}\text{LCu}^{\text{I}}$  at  $-325 \text{ mV}$ , and their peak-to-peak separation was also about the same,  $\Delta E_{\text{avg}} = 115 \text{ mV}$ . These results suggest that the steric influence of the quinoline donor is similar to that of the 6-*t*-butyl substituent. The same  $E_{1/2}$  values were also measured for  $^{\text{Im}}\text{LCu}^{\text{I}}$  and  $^{\text{NMe}_2}\text{LCu}^{\text{I}}$  at  $-445 \text{ mV}$ , which was surprising because of their different static copper(II) structures. The X-ray crystal structure of  $[\text{Cu}^{\text{II}}(\text{NMe}_2\text{L})(\text{Cl})]^{2+}$  reveals a distorted square pyramidal coordination geometry,  $\tau = 0.26$ .<sup>62,86</sup> The  $\tau$  structural parameter is 0.00 for a perfect square pyramidal structure and 1.00 for a perfect trigonal bipyramidal coordination geometry.<sup>86,87</sup> By contrast,  $[\text{Cu}^{\text{II}}(^{\text{Im}}\text{L})(\text{CH}_3\text{CN})]^{2+}$  displays a trigonal bipyramidal static structure,  $\tau = 0.86$ .<sup>65,86</sup>

Since  $[\text{Cu}^{\text{II}}(^{\text{Py}}\text{L})(\text{CH}_3\text{CN})]^{2+}$  has an almost perfect trigonal bipyramidal static structure,  $\tau = 0.96$ ,<sup>67,86</sup> the same degree of structural rearrangement would be expected to occur upon oxidation of  $^{\text{Im}}\text{LCu}^{\text{I}}$  and  $^{\text{Py}}\text{LCu}^{\text{I}}$ . Both of their cuprous–acetonitrile structures are assumed to be very similar based on their related  $^{\text{D}}\text{LCu}^{\text{I}}\text{-CO}$   $^4\nu_{\text{CO}}$  values. However, the  $E_{1/2}$  values are quite different for  $^{\text{Im}}\text{LCu}^{\text{I}}$  ( $107 \text{ mV}$ ) and  $^{\text{Py}}\text{LCu}^{\text{I}}$  ( $76 \text{ mV}$ ), suggesting that the *in situ* copper(II) structures are different. The  $E_{1/2}$  value of  $^{\text{Im}}\text{LCu}^{\text{I}}$  (and  $^{\text{NMe}_2}\text{LCu}^{\text{I}}$ ) in comparison to  $^{\text{Py}}\text{LCu}^{\text{I}}$  ( $-410 \text{ mV}$ ) is  $35 \text{ mV}$  more negative; therefore, the latter is easier to reduce.

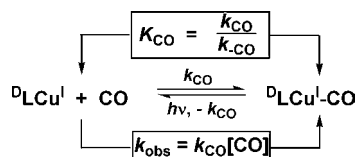
**CO Equilibrium Binding and Thermodynamic Parameters ( $K_{\text{CO}}$ ,  $\Delta H^\circ$ ,  $\Delta S^\circ$ ).** The equilibrium CO binding constants ( $K_{\text{CO}}$ , Scheme 1) and corresponding thermodynamic parameters ( $\Delta H^\circ$ ,  $\Delta S^\circ$ ) were determined by variable-temperature monitoring of

- (83) Carrier, S. M.; Ruggiero, C. E.; Houser, R. P.; Tolman, W. B. *Inorg. Chem.* **1993**, *32*, 4889–4899.
- (84) Hu, Z. B.; Williams, R. D.; Tran, D.; Spiro, T. G.; Gorun, S. M. *J. Am. Chem. Soc.* **2000**, *122*, 3556–3557.
- (85) Zhang, C. X.; Liang, H. C.; Kim, E. I.; Shearer, J.; Helton, M. E.; Kim, E.; Kaderli, S.; Incarvito, C. D.; Zuberhuhler, A. D.; Rheingold, A. L.; Karlin, K. D. *J. Am. Chem. Soc.* **2003**, *125*, 634–635.
- (86)  $\tau$  values ( $\alpha\text{-}\beta/60^\circ$ ) calculated on the basis of the X-ray crystallographic data reported in cited references.
- (87) Addison, A. W.; Rao, T. N.; Reedijk, J.; Vanrijn, J.; Verschoor, G. C. *J. Chem. Soc., Dalton Trans.* **1984**, 1349–1356.

**Table 2.** Kinetic and Thermodynamic Parameters for CO binding to <sup>D</sup>LCu<sup>I</sup> in THF<sup>a</sup>

compound	$K_{\text{CO}}$ (M <sup>-1</sup> )	$\Delta H^\ddagger$	$\Delta S^\ddagger$	$k_{\text{CO}}$ (M <sup>-1</sup> s <sup>-1</sup> )	$\Delta H^\ddagger$	$\Delta S^\ddagger$	$k_{-\text{CO}}$ (s <sup>-1</sup> )	$\Delta H^\ddagger$	$\Delta S^\ddagger$
<sup>Im</sup> LCu <sup>I</sup> -CO	$(2.4 \pm 0.04) \times 10^3$	-31.4	-40.6	$(2.8 \pm 0.07) \times 10^9$	7.03	-40.5	$(1.1 \pm 0.04) \times 10^6$	38.5	0.1
<sup>NMe<sub>2</sub></sup> LCu <sup>I</sup> -CO	$(5.0 \pm 0.05) \times 10^3$	-39.7	-62.5	$(2.5 \pm 0.05) \times 10^9$	9.07	-34.7	$(5.0 \pm 0.09) \times 10^5$	48.8	28
<sup>Py</sup> LCu <sup>I</sup> -CO	$(1.2 \pm 0.05) \times 10^4$	-35.9	-42.6	$(1.9 \pm 0.02) \times 10^9$	7.13	-43.3	$(1.5 \pm 0.04) \times 10^5$	43.0	-0.7
<sup>Q</sup> LCu <sup>I</sup> -CO	$(2.2 \pm 0.2) \times 10^4$	-39.2	-48.5	$(9.7 \pm 0.1) \times 10^8$	5.66	-53.9	$(4.4 \pm 0.01) \times 10^4$	44.9	-5.3
<sup>TBP</sup> LCu <sup>I</sup> -CO	$(1.4 \pm 0.03) \times 10^4$	-40.4	-56.2	$(5.2 \pm 0.01) \times 10^8$	5.76	-58.7	$(3.7 \pm 0.01) \times 10^4$	46.2	-2.5
<sup>B<sup>z</sup></sup> LCu <sup>I</sup> -CO	$(5.6 \pm 0.1) \times 10^4$	-46.0	-63.6	$(5.0 \pm 0.01) \times 10^8$	0.74	-75.9	$(9.0 \pm 0.03) \times 10^3$	46.8	-76

<sup>a</sup> Constants reported at 298 K. Units of kinetic and thermodynamic values are as follows:  $K_{\text{CO}}$ , M<sup>-1</sup>;  $k_{\text{CO}}$ , M<sup>-1</sup> s<sup>-1</sup>;  $k_{-\text{CO}}$ , s<sup>-1</sup>;  $\Delta H^\ddagger$ , kJ mol<sup>-1</sup>;  $\Delta S^\ddagger$ , J mol<sup>-1</sup> K<sup>-1</sup>. See Supporting Information for Van't Hoff and Eyring plots.

**Scheme 1**

reactions of CO with <sup>D</sup>LCu<sup>I</sup> to form <sup>D</sup>LCu<sup>I</sup>-CO in THF solvent.<sup>59</sup> Throughout the entire series (Table 2),  $K_{\text{CO}}$  increases are accompanied by decreasing (more favorable) enthalpies but less favorable (decreasing) reaction entropies. This behavior is typical, as enhanced binding can be described as being “tighter”. UV–visible spectral data representative of the conversion of <sup>TBP</sup>LCu<sup>I</sup> to <sup>TBP</sup>LCu<sup>I</sup>-CO are shown in Figure 4; data corresponding to all other species are found in the Supporting Information.

**CO Photodissociation and Rebinding Kinetics.** The kinetics and thermodynamics of CO binding to <sup>D</sup>LCu<sup>I</sup> were measured through variable-temperature (20 to -80 °C) TA laser flash photolysis experiments.<sup>15,59</sup> Absorption difference spectra,  $\text{Abs}\{[\text{D}^{\text{I}}\text{LCu}^{\text{I}}] - [\text{D}^{\text{I}}\text{LCu}^{\text{I}}\text{-CO}]\}$ , calculated from steady-state absorption experiments were in agreement with observed transient data collected within the range  $\lambda_{\text{mon}} = 325\text{--}700$  nm; see Figure 5 for  $\Delta A$  spectra corresponding to photodissociation of CO from <sup>TBP</sup>LCu<sup>I</sup>-CO. The subsequent rebinding of CO followed a first-order kinetic model. Bimolecular rate constants ( $k_{\text{CO}}$ ) for <sup>D</sup>LCu<sup>I</sup>-CO formation were calculated on the basis of [CO] dependence studies.<sup>59</sup> Complementary activation ( $\Delta H^\ddagger$ ,  $\Delta S^\ddagger$ ) parameters were calculated by determination of  $k_{\text{CO}}$  at variable temperatures and through Eyring analysis.<sup>59</sup>

In all cases, CO (re)binding to <sup>D</sup>LCu<sup>I</sup> follows an associative mechanism as suggested by the  $k_{\text{CO}}$  associated negative reaction entropies ( $\Delta S^\ddagger$ ) in the range -40 to -76 J mol<sup>-1</sup> K<sup>-1</sup> (see Table 2). Furthermore, the nearly identical thermodynamic ( $\Delta S^\ddagger$ ) and

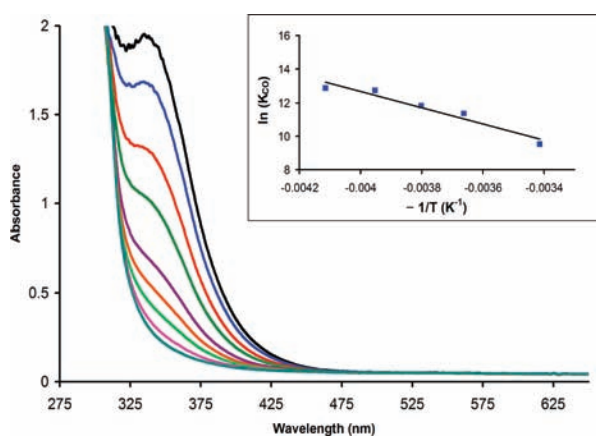


**Figure 4.** Spectrophotometric titration of CO to <sup>TBP</sup>LCu<sup>I</sup> in THF at room temperature. The inset is a Van't Hoff plot of the variable-temperature  $K_{\text{CO}}$  data collected from -30 to +20 °C.

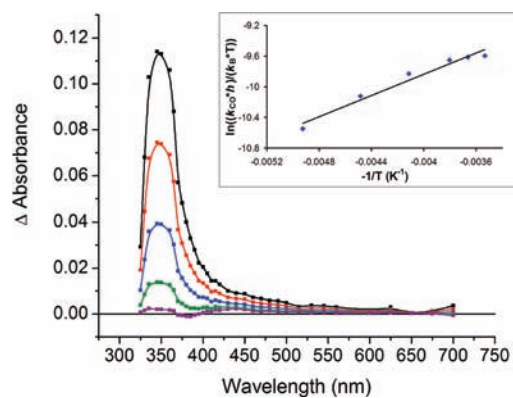


**Figure 5.** Transient absorption difference spectra observed after pulsed 355 nm excitation of <sup>TBP</sup>LCu<sup>I</sup>-CO in THF at room temperature under 1 atm of CO. CO photodissociation and the formation of <sup>TBP</sup>LCu<sup>I</sup> followed by subsequent CO recombination are measured and shown at various delay times: 0 (black), 100 (red), 250 (blue), 500 (green), and 1000 ns (purple). The inset is an Eyring analysis plot of the  $k_{\text{CO}}$  data collected at variable temperatures (-70 to 10 °C).

activation ( $\Delta S^\ddagger$ ) entropies along the <sup>D</sup>L series of complexes suggest a late transition state; the rate-determining step involves an intermediate that is structurally similar to the final carbonylated product. Following CO photodissociation, the dangling N-donor arm of <sup>D</sup>LCu<sup>I</sup>-CO binds to the open coordination site of the cuprous ion and must dissociate before CO can rebind.

**Thermal <sup>D</sup>LCu<sup>I</sup>-CO Dissociation Kinetics.** With  $K_{\text{CO}}$  and  $k_{\text{CO}}$  values determined experimentally, the thermal CO dissociation rate constants ( $k_{-\text{CO}}$ ) and corresponding activation parameters ( $\Delta H^\ddagger$ ,  $\Delta S^\ddagger$ ) were calculated.<sup>59</sup> As expected, the  $k_{-\text{CO}}$  value increases with decreasing reaction enthalpies ( $\Delta H^\ddagger$ ) and increasing entropic ( $\Delta S^\ddagger$ ) values. The transition state largely correlates with the overall geometry change as related to the degree to which the dangling arm is or is not interacting with the cuprous–carbonyl upon Cu–C bond breakage. See below for further discussion.

**Kinetics ( $k_{\text{O}_2}$ ,  $\Delta H^\ddagger$ ,  $\Delta S^\ddagger$ ) in THF of 1:1 Dioxygen Binding to <sup>D</sup>LCu<sup>I</sup> following CO Photodissociation from <sup>D</sup>LCu<sup>I</sup>-CO (D = Py, Im, NMe<sub>2</sub>).** The primary interaction (1:1) of O<sub>2</sub> with <sup>Py</sup>LCu<sup>I</sup>, <sup>Im</sup>LCu<sup>I</sup>, and <sup>NMe<sub>2</sub></sup>LCu<sup>I</sup> to form <sup>D</sup>LCu<sup>II</sup>-O<sub>2</sub><sup>-</sup> was monitored and measured in THF solvent through the “flash-and-trap” method.<sup>15</sup> The experiments were conducted in the presence of precisely determined concentrations of O<sub>2</sub> and CO within the temperature range of -55 to -85 °C on nanosecond and longer time scales. The  $\Delta A$  spectra,  $\text{Abs}\{[\text{NMe}_2\text{LCu}^{\text{I/II}}\text{-X}] - [\text{NMe}_2\text{LCu}^{\text{I}}\text{-CO}]\}$  (X = THF or O<sub>2</sub><sup>-</sup>), representing the two separate O<sub>2</sub>-binding processes ( $k_{\text{fast}}$ ,  $k_{\text{slow}}$ ) for formation of <sup>NMe<sub>2</sub></sup>LCu<sup>II</sup>-O<sub>2</sub><sup>-</sup> are shown in Figure 6; corresponding data for formation of <sup>Im</sup>LCu<sup>II</sup>-O<sub>2</sub><sup>-</sup> are given in the Supporting Information. As depicted in Scheme 2, the initial “fast” process ( $k_{\text{fast}}$ , Figure 6A) involves the competitive binding of both CO and O<sub>2</sub> with <sup>D</sup>LCu<sup>I</sup>, either regenerating <sup>D</sup>LCu<sup>I</sup>-CO or forming <sup>D</sup>LCu<sup>II</sup>-O<sub>2</sub><sup>-</sup>; thus,  $k_{\text{fast}}$  is a

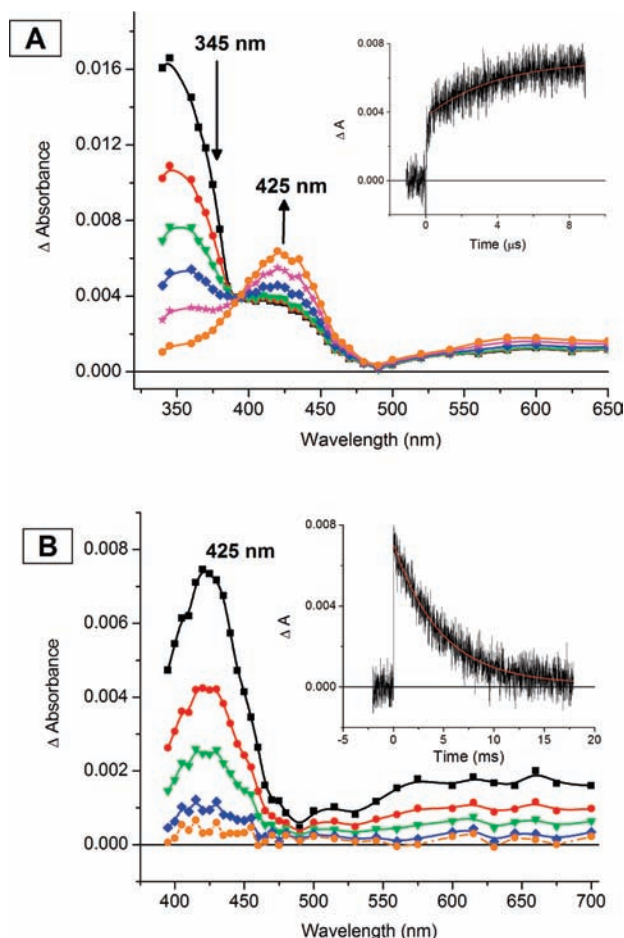
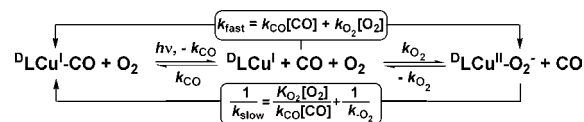


**Figure 6.** Absorption difference spectra [ $\text{NMe}_2\text{LCu}^{\text{II}}\text{-X} - \text{NMe}_2\text{LCu}^{\text{I}}\text{-CO}$ ] recorded after pulsed  $\lambda_{\text{ex}} = 355$  nm excitation of  $\text{NMe}_2\text{LCu}^{\text{I}}\text{-CO}$  in THF at 193 K under 1 atm  $\text{O}_2\text{:CO}$  (1:1) mixture. The spectra were recorded at various delay times: (A) 0–5  $\mu\text{s}$ , representing the conversion of  $\text{NMe}_2\text{LCu}^{\text{I}}$  to a mixture of  $\text{NMe}_2\text{LCu}^{\text{I}}\text{-CO}$  and  $\text{NMe}_2\text{LCu}^{\text{II}}\text{-O}_2^-$  (black squares, 0  $\mu\text{s}$ ; red circles, 0.1  $\mu\text{s}$ ; green triangles, 0.25  $\mu\text{s}$ ; blue diamonds, 1  $\mu\text{s}$ ; magenta stars, 2.5  $\mu\text{s}$ ; orange circles, 5.0  $\mu\text{s}$ ). The inset is an absorption transient monitored at 425 nm with a superimposed first-order fit (in red),  $k_{\text{obs}} = 2.92 \times 10^5 \text{ s}^{-1}$ . (B) 0–20 ms, representing the conversion from  $\text{NMe}_2\text{LCu}^{\text{II}}\text{-O}_2^-$  to  $\text{NMe}_2\text{LCu}^{\text{I}}\text{-CO}$  (black squares, 0 ms; red circles, 2.5 ms; green triangles, 5.0 ms; blue diamonds, 10 ms; orange circles, 20 ms). The inset is an absorption transient monitored at 425 nm with a superimposed first-order fit (in red),  $k_{\text{obs}} = 236 \text{ s}^{-1}$ .

combination of two rate constants,  $k_{\text{O}_2}$  and  $k_{\text{CO}}$ . Following generation of  $\text{DLCu}^{\text{II}}\text{-O}_2^-$ , since  $K_{\text{CO}} \gg K_{\text{O}_2}$ , CO subsequently displaces coordinated  $\text{O}_2$  to re-form the initial  $\text{DLCu}^{\text{I}}\text{-CO}$  species ( $k_{\text{slow}}$ ). The latter values,  $k_{\text{O}_2}$  (and  $K_{\text{O}_2}$  and  $k_{-\text{O}_2}$ ) derived from  $k_{\text{slow}}$ , are tabulated here and used for discussion.

A full analysis of the  $\text{O}_2$  binding kinetics and thermodynamics for formation of  $\text{PyLCu}^{\text{II}}\text{-O}_2^-$  was reported previously in THF solvent via the “flash-and-trap” method,<sup>15</sup> and in EtCN through stopped-flow UV–visible spectroscopy.<sup>8</sup> In the present work, analogous data for formation of  $\text{ImLCu}^{\text{II}}\text{-O}_2^-$  and  $\text{NMe}_2\text{LCu}^{\text{II}}\text{-O}_2^-$  in THF are discussed and compared to those for  $\text{PyLCu}^{\text{II}}\text{-O}_2^-$ . Room-temperature  $k_{\text{O}_2}$  values were obtained by extrapolation from the activation parameters obtained at low temperatures where experimental data could be collected. All data here are also compared to those obtained by Schindler, Zuberbühler, and co-workers on the closely related tripodal tetradentate ligand complex  $[\text{Cu}^{\text{I}}(\text{Me}_6\text{tren})]^+ \{\text{tris}(2\text{-dimethylaminoethyl})\text{amine}\}^{\text{62}}$  (see Table 3). In fact, very fast reactions with  $k_{\text{O}_2} > 10^7 \text{ M}^{-1}\text{s}^{-1}$  at 298 K have only been observed and determined for the

### Scheme 2



$\text{DLCu}^{\text{I}}$  complexes described here, which includes the previously studied  $\text{PyLCu}^{\text{I}}$  and  $[\text{Cu}^{\text{I}}(\text{Me}_6\text{tren})]^+$  complexes.<sup>13–15</sup>

### Discussion

**CO Equilibrium Binding and Thermodynamic Parameters ( $K_{\text{CO}}$ ,  $\Delta H^\circ$ ,  $\Delta S^\circ$ ).** The  $K_{\text{CO}}$  values for formation of  $\text{DLCu}^{\text{I}}\text{-CO}$  increase as the  $E_{1/2}$  values become more positive and the  ${}^4\nu_{\text{CO}}$  values shift to higher energy (Tables 1 and 2). In previous work that examined the CO binding properties of copper(I)–carbonyl adducts of the R– $\text{PyL}$  ligand series where only electronic effects are present, the opposite trend was observed; thus, a ligand having better donor properties led to enhanced CO binding.<sup>59</sup> This suggests that steric constraints or structural differences induced by changing the dangling “D” N-donor moiety of  $\text{DL}$  significantly affect the  $K_{\text{CO}}$  values in the present systems.

We suggest that the differences in  $\Delta S^\circ$  values or degree of disorder in the reaction are affiliated in part with the extent that the dangling “D” N-donor moiety is interacting with the final  $\text{DLCu}^{\text{I}}\text{-CO}$  adduct. For example, the  $\text{Cu}^{\text{I}}\text{-CO}$  adduct of the purely tridentate  $\text{BzL}$  has the highest  $K_{\text{CO}}$  value of  $5.6 \times 10^4 \text{ M}^{-1}$ . This clearly derives from  $\text{BzLCu}^{\text{I}}\text{-CO}$  having the most favorable reaction enthalpy in the series,  $\Delta H^\circ = -46.0 \text{ kJ mol}^{-1} \text{ K}^{-1}$ , since the reaction is the most disfavored entropically,  $\Delta S^\circ = -63.6 \text{ kJ mol}^{-1} \text{ K}^{-1}$ . In more depth, formation of  $\text{BzLCu}^{\text{I}}\text{-CO}$  is the most ordered reaction, meaning the benzyl D-group does not coordinate or donate any significant electron density to the cuprous center and also does not hinder coordination of CO to  $\text{BzLCu}^{\text{I}}$ .

The  $K_{\text{CO}}$  values for CO binding to  $\text{QLCu}^{\text{I}}$  and  $\text{TBPLCu}^{\text{I}}$  are the highest of the tetradentate ligands studied,  $2.2 \times 10^4$  and  $1.4 \times 10^4 \text{ M}^{-1}$ , respectively. Based on their solution and solid-state  ${}^4\nu_{\text{CO}}$  values, the ligand–copper(I)–carbonyl complexes of both are tridentate in nature, consistent with the X-ray crystal structure of  $\text{TBPLCu}^{\text{I}}\text{-CO}$  (*vide supra*). However, in comparison to  $\text{BzLCu}^{\text{I}}\text{-CO}$ , the coordination of CO to the cuprous ion of  $\text{QLCu}^{\text{I}}$  and  $\text{TBPLCu}^{\text{I}}$  must be somewhat hindered by their bulky “D” N-donor groups (i.e., quinolyl or  $t\text{-Bu}$ -pyridyl arms), resulting in their slightly lower  $K_{\text{CO}}$  values (Table 2).

At the low end of the range, reaction of  $\text{ImLCu}^{\text{I}}$  with CO results in the smallest  $K_{\text{CO}}$  value of  $2.4 \times 10^3 \text{ M}^{-1}$  with the most favorable entropy,  $\Delta S^\circ = -40.6 \text{ kJ mol}^{-1} \text{ K}^{-1}$ . We suggest that the dangling imidazole is more interacting with the cuprous–carbonyl center, resulting in increased disorder. The bond enthalpy for formation of  $\text{ImLCu}^{\text{I}}\text{-CO}$  is the highest ( $\Delta H^\circ = -31.4 \text{ kJ mol}^{-1}$ ), consistent with the weakest Cu–C bond of the series.

In comparison to the reaction of CO with  $\text{PyLCu}^{\text{I}}$ , the  $K_{\text{CO}}$  value of  $1.2 \times 10^4 \text{ M}^{-1}$  is approximately 5 times higher as a result of the slightly lower thermodynamic values,  $\Delta H^\circ = -35.9 \text{ kJ mol}^{-1}$ ,  $\Delta S^\circ = -42.6 \text{ kJ mol}^{-1} \text{ K}^{-1}$ .<sup>59</sup> Such small differences in the thermodynamic parameters, yet large effect on the equilibrium CO binding constant, may suggest that the dangling pyridyl arm of  $\text{PyL}$  is less interacting with the cuprous ion than is the imidazolyl moiety of  $\text{ImL}$ .

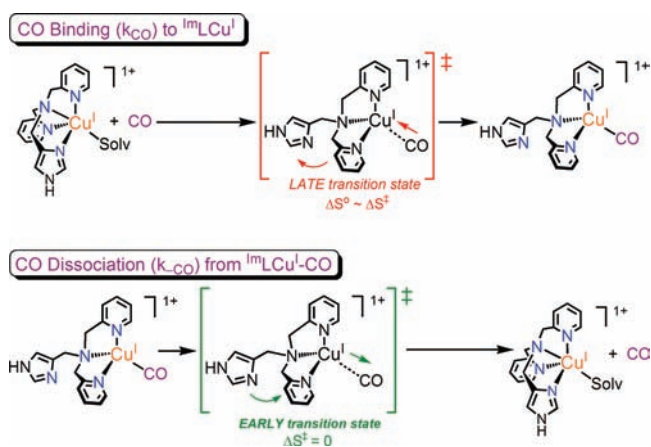
By contrast, the equilibrium binding constant of  $K_{\text{CO}} = 5.0 \times 10^3 \text{ M}^{-1}$  for reaction of CO with  $\text{NMe}_2\text{LCu}^{\text{I}}$  is lower. However, the highly negative  $\Delta S^\circ$  value of  $-62.5 \text{ kJ mol}^{-1} \text{ K}^{-1}$  is similar



**Table 3.** Comparison of the Kinetics and Thermodynamics for Formation of <sup>D</sup>LCu<sup>I</sup>–O<sub>2</sub><sup>−</sup> (D = Py, Im, NMe<sub>2</sub>) in THF and Other Ligand–Copper(II)–η<sup>1</sup>-Superoxo Species

	parameter	<sup>Py</sup> LCu <sup>I</sup> in THF <sup>a</sup>	<sup>Py</sup> LCu <sup>I</sup> in EtCN <sup>b</sup>	[Cu <sup>I</sup> (Me <sub>6</sub> tren)] <sup>+</sup> in EtCN <sup>b</sup>	<sup>Im</sup> LCu <sup>I</sup> in THF <sup>c</sup>	<sup>NMe<sub>2</sub></sup> LCu <sup>I</sup> in THF <sup>c</sup>
<i>k</i> <sub>O<sub>2</sub></sub>	193 K (M <sup>−1</sup> s <sup>−1</sup> )	(1.5 ± 0.02) × 10 <sup>8</sup>	(3.8 ± 0.01) × 10 <sup>4</sup>	(1.8 ± 0.04) × 10 <sup>5</sup>	(1.8 ± 0.03) × 10 <sup>8</sup>	(6.9 ± 0.02) × 10 <sup>7</sup>
<i>k</i> <sub>O<sub>2</sub></sub>	298 K (M <sup>−1</sup> s <sup>−1</sup> )	(1.3 ± 0.02) × 10 <sup>9</sup>	(5.8 ± 0.8) × 10 <sup>7</sup>	(1.2 ± 0.1) × 10 <sup>7</sup>	(3.4 ± 0.6) × 10 <sup>10</sup>	(2.3 ± 0.4) × 10 <sup>11</sup>
	Δ <i>H</i> <sup>‡</sup> (kJ mol <sup>−1</sup> )	7.62	31.6	17.1	23.4	32.1
	Δ <i>S</i> <sup>‡</sup> (J mol <sup>−1</sup> K <sup>−1</sup> )	−45.1	10	−52	35.1	80.1
<i>k</i> <sub>−O<sub>2</sub></sub>	193 K (s <sup>−1</sup> )	240 ± 6	130 ± 1	0.62 ± 0.01	1600 ± 0.05	470 ± 0.02
<i>k</i> <sub>−O<sub>2</sub></sub>	298 K (s <sup>−1</sup> )	(1.3 ± 0.03) × 10 <sup>8</sup>	(1.5 ± 0.2) × 10 <sup>8</sup>	(7.7 ± 0.9) × 10 <sup>5</sup>	(1.9 ± 0.2) × 10 <sup>9</sup>	(2.3 ± 0.3) × 10 <sup>9</sup>
	Δ <i>H</i> <sup>‡</sup> (kJ mol <sup>−1</sup> )	58.0	61.5	62.0	64.5	66.5
	Δ <i>S</i> <sup>‡</sup> (J mol <sup>−1</sup> K <sup>−1</sup> )	105	118	76	150	157
<i>K</i> <sub>O<sub>2</sub></sub>	193 K (M <sup>−1</sup> )	(6.5 ± 0.02) × 10 <sup>5</sup>	260 ± 4	(2.9 ± 0.04) × 10 <sup>5</sup>	(1.1 ± 0.03) × 10 <sup>5</sup>	(1.5 ± 0.06) × 10 <sup>5</sup>
<i>K</i> <sub>O<sub>2</sub></sub>	298 K (M <sup>−1</sup> )	15.4 ± 0.3	0.38 ± 0.02	15.5 ± 0.5	17.4 ± 0.8	100 ± 0.7
	Δ <i>H</i> <sup>°</sup> (kJ mol <sup>−1</sup> )	−48.5	−29.8	−44.9	−41.1	−34.4
	Δ <i>S</i> <sup>°</sup> (J mol <sup>−1</sup> K <sup>−1</sup> )	−140	−108	−128	−114	−77.3

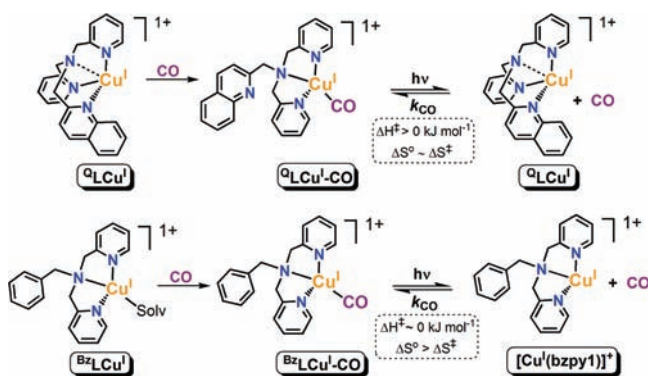
<sup>a</sup> O<sub>2</sub> binding data were previously published and collected through flash-and-trap techniques in THF.<sup>15</sup> <sup>b</sup> O<sub>2</sub> binding data were previously published and collected through stopped-flow spectroscopy in EtCN.<sup>14,85</sup> <sup>c</sup> Averaged values were determined from analysis of *k*<sub>slow</sub> using the flash-and-trap methods discussed herein; see text for more details. Bimolecular *k*<sub>O<sub>2</sub></sub> values calculated at additional temperatures are given in the Supporting Information, Table S2.

**Scheme 3**

to that of <sup>Bz</sup>LCu<sup>I</sup>–CO, suggesting that the aliphatic dimethylamino arm is barely interacting, if at all, with the cuprous ion of <sup>NMe<sub>2</sub></sup>LCu<sup>I</sup> *in situ*. Such a characteristic is consistent with the absence of an observable <sup>5</sup>ν<sub>CO</sub> stretch for <sup>NMe<sub>2</sub></sup>LCu<sup>I</sup>–CO.

**CO Photodissociation and Rebinding Kinetics.** The rate constant for formation of <sup>D</sup>LCu<sup>I</sup>–CO (*k*<sub>CO</sub>) appears to be controlled by the degree to which the dangling “D” arm interacts with the cuprous ion during Cu–C bond formation. This conclusion comes about from the observation that decreasing <sup>4</sup>ν<sub>CO</sub> frequencies for <sup>D</sup>LCu<sup>I</sup>–CO along with decreased complex *E*<sub>1/2</sub> values for <sup>D</sup>LCu<sup>I</sup>, which both indicate a better donor ligand, correlate with an increase in *k*<sub>CO</sub> values (Tables 1 and 2). For example, <sup>Im</sup>LCu<sup>I</sup>–CO is comprised of the most electron-donating N-donor system for copper(I) due to the presence of the imidazolyl donor moiety, and this complex gives the highest rate constant, *k*<sub>CO</sub> = 2.8 × 10<sup>9</sup> M<sup>−1</sup> s<sup>−1</sup>. The corresponding activation parameters for formation of <sup>Im</sup>LCu<sup>I</sup>–CO, Δ*H*<sup>‡</sup> = 7.03 kJ mol<sup>−1</sup> and Δ*S*<sup>‡</sup> = −40.5 kJ mol<sup>−1</sup> K<sup>−1</sup>, are very similar to those measured for <sup>Py</sup>LCu<sup>I</sup>–CO, suggesting little differences in the CO coordination dynamics. The coordination of CO to <sup>Im</sup>LCu<sup>I</sup> is depicted in Scheme 3.

Consistent with the nearly equivalent *E*<sub>1/2</sub> values determined for <sup>Im</sup>LCu<sup>I</sup> and <sup>NMe<sub>2</sub></sup>LCu<sup>I</sup>, <sup>NMe<sub>2</sub></sup>LCu<sup>I</sup>–CO has a similar CO rebinding rate of 2.5 × 10<sup>9</sup> M<sup>−1</sup> s<sup>−1</sup>. However, the Δ*S*<sup>‡</sup> value affiliated with CO binding to <sup>NMe<sub>2</sub></sup>LCu<sup>I</sup> is much more positive than the Δ*S*<sup>°</sup> value, suggesting that the course of reaction is more disordered as a result of the dangling or

**Scheme 4**

very weakly interacting donor moiety. Unlike for <sup>Im</sup>LCu<sup>I</sup>–CO and <sup>Py</sup>LCu<sup>I</sup>–CO, a five-coordinate carbonyl species is not structurally favorable for <sup>NMe<sub>2</sub></sup>LCu<sup>I</sup>–CO; in support of this supposition, note that only a <sup>4</sup>ν<sub>CO</sub> value was observed, *vide supra*. As a result, dissociation of the fourth ligand N-donor arm of <sup>NMe<sub>2</sub></sup>LCu<sup>I</sup> followed by subsequent CO rebinding likely involves significant structural changes, resulting in a higher Δ*S*<sup>‡</sup> value.

The parallel thermodynamic and activation parameters associated with CO binding to <sup>QL</sup>Cu<sup>I</sup> (9.7 × 10<sup>8</sup> M<sup>−1</sup> s<sup>−1</sup>) and <sup>TBp</sup>LCu<sup>I</sup> (5.2 × 10<sup>8</sup> M<sup>−1</sup> s<sup>−1</sup>) suggest that the mechanism of reaction is the same for both (Scheme 4). Such similarities are consistent with their analogous <sup>4</sup>ν<sub>CO</sub> values and identical *E*<sub>1/2</sub> values. Since solvent (THF) does not coordinate to <sup>QL</sup>Cu<sup>I</sup> and <sup>TBp</sup>LCu<sup>I</sup>, only the “D” N-donor must dissociate from the cuprous ion to form their respective ligand–copper(I)–carbonyl adducts.

Carbon monoxide rebinding to <sup>Bz</sup>LCu<sup>I</sup>, where a fourth endogenous N-donor is not present, results in the lowest *k*<sub>CO</sub> value of 5.0 × 10<sup>8</sup> M<sup>−1</sup> s<sup>−1</sup>; note that this species exhibits the most positive *E*<sub>1/2</sub> value. The negligible enthalpy (Δ*H*<sup>‡</sup> = 0.74 kJ mol<sup>−1</sup>) and highly negative entropy (Δ*S*<sup>‡</sup> = −75.9 J mol<sup>−1</sup> K<sup>−1</sup>) of activation imply that the tridentate nature of <sup>Bz</sup>L minimizes geometric changes in the reaction of CO with <sup>Bz</sup>LCu<sup>I</sup> and that the “dangling” benzyl group does not hamper CO rebinding to the cuprous center. However, since the standard entropy (Δ*S*<sup>°</sup>) for formation of <sup>Bz</sup>LCu<sup>I</sup>–CO is greater than the activation entropy (Δ*S*<sup>‡</sup>), it is possible that the CO molecule rebinds to the naked [Cu<sup>I</sup>(<sup>Bz</sup>L)]<sup>+</sup> species before THF transiently

Scheme 5



coordinates, resulting in a more ordered reaction and negligible enthalpy of activation ( $\Delta H^\ddagger$ ), as shown in Scheme 4.

**Thermal  $^{\text{D}}\text{LCu}^{\text{I}}-\text{CO}$  Dissociation Kinetics.** As shown in Scheme 3 for CO dissociation from  $^{\text{Im}}\text{LCu}^{\text{I}}-\text{CO}$ , the dangling arm ligates to the copper(I) ion following CO dissociation. The negligible activation entropy ( $\Delta S^\ddagger \approx 0 \text{ J mol}^{-1} \text{ K}^{-1}$ ) suggests that there is little overall geometry difference between the initial carbonylated complex and the transition state. Therefore, the increased donation offered by the slightly interacting imidazole in  $^{\text{Im}}\text{LCu}^{\text{I}}-\text{CO}$  results in an overall decrease in the structural changes as well as a decrease in the activation barrier to cleave the Cu–C bond.  $^{\text{Im}}\text{LCu}^{\text{I}}-\text{CO}$  has a  $k_{-\text{CO}}$  value of  $1.1 \times 10^6 \text{ s}^{-1}$ , with a corresponding reaction enthalpy of  $\Delta H^\ddagger = 38.5 \text{ kJ mol}^{-1}$ . Similar characteristics were exhibited by  $^{\text{Py}}\text{LCu}^{\text{I}}-\text{CO}$ ,<sup>59</sup>  $^{\text{Q}}\text{LCu}^{\text{I}}-\text{CO}$ , and  $^{\text{TBP}}\text{LCu}^{\text{I}}-\text{CO}$  for CO dissociation, all with near-zero  $\Delta S^\ddagger$  values (Table 2).

Dissociation of CO from  $^{\text{NMe}_2}\text{LCu}^{\text{I}}-\text{CO}$  is characterized by  $\Delta S^\ddagger = 28 \text{ J mol}^{-1} \text{ K}^{-1}$ , a more favorable value than is observed for any other in the series (Table 2). Thus, Cu–C bond cleavage involves considerable structural rearrangement, and the high  $\Delta S^\ddagger$  value implies an early transition state structurally similar to the terminal copper(I)–carbonyl species. Such a mechanism would require the dimethylamino donor arm of  $^{\text{NMe}_2}\text{L}$  to be predominantly in the unbound state when the Cu–C bond is broken and further suggests that coordination of solvent occurs prior to or concomitant with CO release (see Scheme 5). As already stated, it is unfavorable for the hard dimethylamino arm to interact with the soft cuprous–carbonyl center, as evidenced or supported by a lack of observation of  $\nu_{\text{CO}}$  for  $^{\text{NMe}_2}\text{LCu}^{\text{I}}-\text{CO}$ .

Conversely, dissociation of CO from  $^{\text{Bz}}\text{LCu}^{\text{I}}-\text{CO}$  is accompanied by a strikingly unique unfavorable activation entropy of  $\Delta S^\ddagger = -76 \text{ J mol}^{-1} \text{ K}^{-1}$  that leads to the smallest  $k_{-\text{CO}}$  value ( $9.0 \times 10^3 \text{ s}^{-1}$ ) in the series. The almost identical  $\Delta S^\ddagger$  values for the forward and reverse reaction of  $^{\text{Bz}}\text{LCu}^{\text{I}}/\text{CO}$  suggest that virtually no geometry change results, and therefore the reaction is highly ordered; i.e., there is a late transition state.

**Kinetics ( $k_{\text{O}_2}$ ,  $\Delta H^\ddagger$ ,  $\Delta S^\ddagger$ ) in THF of 1:1 Dioxygen Binding to  $^{\text{D}}\text{LCu}^{\text{I}}$  following CO Photodissociation from  $^{\text{D}}\text{LCu}^{\text{I}}-\text{CO}$  (D = Py, Im, NMe<sub>2</sub>).** An examination of activation parameters ( $\Delta H^\ddagger$ ,  $\Delta S^\ddagger$ ; Table 3) indicates there is a striking difference between those for formation of  $^{\text{Py}}\text{LCu}^{\text{II}}-\text{O}_2^-$  compared to the other two copper(II)– $\eta^1$ -superoxo complexes,  $^{\text{Im}}\text{LCu}^{\text{II}}-\text{O}_2^-$  and  $^{\text{NMe}_2}\text{LCu}^{\text{II}}-\text{O}_2^-$ . The binding of O<sub>2</sub> to  $^{\text{Py}}\text{LCu}^{\text{I}}$  occurs with a relatively large and negative activation entropy ( $-45.1 \text{ J mol}^{-1} \text{ K}^{-1}$ , Table 3), indicating an associative reaction mechanism is involved.<sup>15</sup> This suggests O<sub>2</sub> binds prior to loss of the bound solvent molecule and then THF solvent de-ligates. Or, solvent may not even coordinate to the cuprous center, accounting for a simple (unhindered) association of dioxygen. As an example of the latter point, the tetradentate ligand–copper(I) complex  $[\text{Cu}^{\text{I}}(\text{Me}_6\text{-tren})]^+$  does not coordinate an exogenously derived nitrile ligand.<sup>14</sup> As a result, an associative O<sub>2</sub> binding mechanism ( $\Delta S^\ddagger$

$= -52 \text{ J mol}^{-1} \text{ K}^{-1}$ ) resulted for formation of  $[\text{Cu}^{\text{II}}(\text{Me}_6\text{-tren})(\text{O}_2^-)]^+$  in EtCN (see Table 3). By extreme contrast, the positive activation entropies measured for  $^{\text{NMe}_2}\text{LCu}^{\text{II}}-\text{O}_2^-$  ( $\Delta S^\ddagger = 80.1 \text{ J mol}^{-1} \text{ K}^{-1}$ ) and  $^{\text{Im}}\text{LCu}^{\text{II}}-\text{O}_2^-$  ( $\Delta S^\ddagger = 35.1 \text{ J mol}^{-1} \text{ K}^{-1}$ ) indicate that the O<sub>2</sub> binding reaction follows a dissociative mechanism where de-ligation of solvent (THF) occurs prior to O<sub>2</sub> binding. Throughout the remainder of the text, this latter reaction mechanism is referred to as a dissociative process; however, we note that a purely dissociative mechanism would result in first-order kinetics. Therefore, it is perhaps more appropriate to describe this process as a dissociative interchange reaction, in which bond breakage dominates over bond formation. A more detailed explanation and analysis of the dioxygen binding mechanisms is given below.

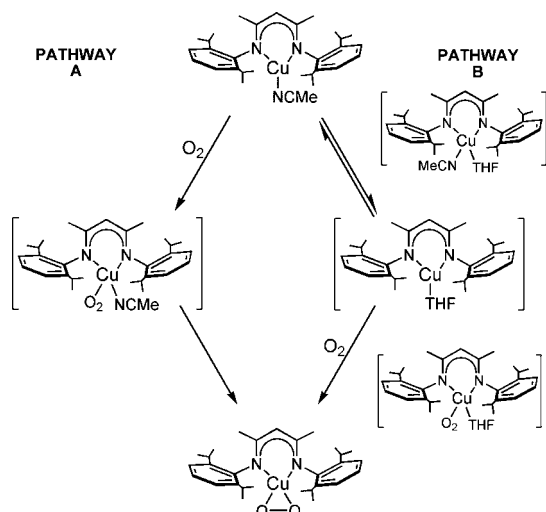
As discussed earlier in the text, the structurally characterized cupric chloride species  $[\text{NMe}_2\text{LCu}^{\text{II}}(\text{Cl})]^+$  has a square pyramidal geometry ( $\tau = 0.26$ ),<sup>62</sup> different than the trigonal bipyramidal structures exhibited by  $[\text{PyLCu}^{\text{II}}(\text{Cl})]^+$  ( $\tau = 1.00$ ),<sup>88</sup>  $[\text{PyLCu}^{\text{II}}(\text{CH}_3\text{CN})]^{2+}$  ( $\tau = 0.96$ ),<sup>67</sup> and  $[\text{ImLCu}^{\text{II}}(\text{CH}_3\text{CN})]^{2+}$  ( $\tau = 0.86$ ).<sup>65,86</sup> Also, the complementary ligand–copper(I)–CH<sub>3</sub>CN structures of the three aforementioned species  $^{\text{D}}\text{LCu}^{\text{I}}$  have analogous trigonal bipyramidal geometries. Therefore, based on the assumption that the cupric–superoxo species are analogous in structure to their X-ray crystallographically characterized copper(II) adducts, the structural rearrangement that results upon redox changes in the  $^{\text{NMe}_2}\text{L}$  ligand system would be much greater. Consistent with this supposition is the observed highly positive activation entropy,  $\Delta S^\ddagger = 80.1 \text{ kJ mol}^{-1}$ , for the reaction of O<sub>2</sub> with  $^{\text{NMe}_2}\text{LCu}^{\text{I}}$ . Also, the overall redox process, i.e., O<sub>2</sub> binding, results in a higher enthalpy of activation,  $\Delta H^\ddagger = 32.1 \text{ kJ mol}^{-1}$ . The more favorable activation enthalpy for O<sub>2</sub> binding to  $^{\text{Im}}\text{LCu}^{\text{I}}$  ( $\Delta H^\ddagger = 23.4 \text{ kJ mol}^{-1}$ ) and less favorable  $\Delta S^\ddagger$  ( $35.1 \text{ kJ mol}^{-1}$ ) in comparison to  $^{\text{NMe}_2}\text{LCu}^{\text{I}}$  are consistent with a smaller geometry change with copper redox state due to O<sub>2</sub> binding.

**Solvent Dependence (EtCN vs THF) of 1:1 Copper–Dioxygen Adducts.** The dynamics of the O<sub>2</sub> binding reaction of  $^{\text{Py}}\text{LCu}^{\text{I}}$  are largely influenced by solvent medium based on the analogous O<sub>2</sub> binding data collected through the “flash-and-trap” method in THF<sup>15</sup> and stopped-flow UV–visible spectroscopy in EtCN<sup>8</sup> (see Table 3). The entropy of activation ( $\Delta S^\ddagger$ ) for formation of  $^{\text{Py}}\text{LCu}^{\text{II}}-\text{O}_2^-$  in EtCN ( $\Delta S^\ddagger = 10 \text{ J mol}^{-1} \text{ K}^{-1}$ ) versus THF ( $\Delta S^\ddagger = -45.1 \text{ J mol}^{-1} \text{ K}^{-1}$ ) indicates that O<sub>2</sub> binding to  $^{\text{Py}}\text{LCu}^{\text{I}}$  follows a dissociative versus associative pathway, respectively, depending on the solvent. To observe such a solvent effect is not an unreasonable expectation since nitrile solvents are strong Lewis bases and soft donors, therefore strong ligands for copper(I) ions. In some cases, nitrile solvents severely inhibit binding of dioxygen, such as in the reaction of O<sub>2</sub> with  $^{\text{Bz}}\text{LCu}^{\text{I}}$ , where EtCN solvent prevents formation of the commonly observed O<sub>2</sub> adduct, characterized as a dicopper(III)–bis- $\mu$ -oxo species in less coordinating solvents (THF, acetone, toluene).<sup>60</sup>

Previously, Schindler and co-workers attempted to time-resolve the formation of the cupric superoxo species  $^{\text{NMe}_2}\text{LCu}^{\text{II}}-\text{O}_2^-$ .<sup>62</sup> However, the formation was too fast to be measured by stopped-flow UV–visible spectroscopy, even in EtCN (coordinating solvent) at 183 K. Similarly, we have unsuccessfully attempted to measure the formation of  $^{\text{Im}}\text{LCu}^{\text{II}}-\text{O}_2^-$  by stopped-flow methods in EtCN.<sup>65</sup> Conversely, the  $k_{\text{O}_2}$  value for O<sub>2</sub>

(88) Karlin, K. D.; Hayes, J. C.; Juen, S.; Hutchinson, J. P.; Zubieta, J. *Inorg. Chem.* **1982**, *21*, 4106–4108.

Scheme 6

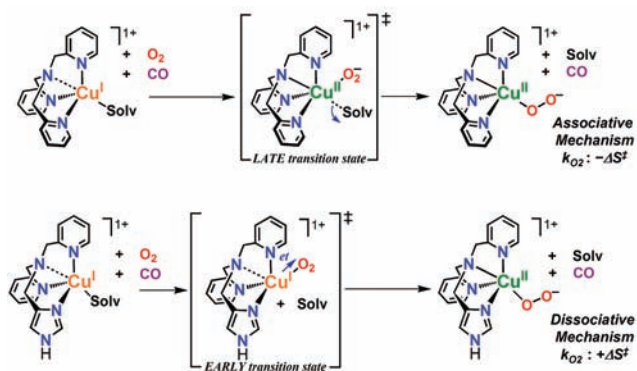


binding to  $\text{PyLCu}^{\text{I}}$  in EtCN was easily measured (Table 3). These comparisons suggest a much higher  $k_{\text{O}_2}$  value in EtCN for formation of  $^{\text{NMe}_2}\text{LCu}^{\text{II}}\text{-O}_2^-$  and  $^{\text{Im}}\text{LCu}^{\text{II}}\text{-O}_2^-$  as compared to  $^{\text{Py}}\text{LCu}^{\text{II}}\text{-O}_2^-$ , as was found for the  $k_{\text{O}_2}$  measurements in THF. Such measurements for formation of  $^{\text{NMe}_2}\text{LCu}^{\text{II}}\text{-O}_2^-$  and  $^{\text{Im}}\text{LCu}^{\text{II}}\text{-O}_2^-$  in EtCN were not carried out, but the values of  $k_{\text{O}_2}$  reported here in THF through the present “flash-and-trap” experiment indeed are very large ( $>6.9 \times 10^7 \text{ M}^{-1} \text{ s}^{-1}$  at 193 K; see Table 3), above the limit of stopped-flow UV–visible spectroscopic methods (millisecond time scale).

THF is usually considered a weakly coordinating solvent for ligand–copper species and has even been described as a non-coordinating solvent. However, THF contains an electron pair centered on the oxygen atom potentially capable of binding to copper(I) or any Lewis acid. A series of ligand–copper(II)–peroxo complexes utilizing the tridentate ligand R–MePY2 (where MePY2 = bis[2-(2-pyridyl)ethyl]methylamine and R = Cl, H, MeO, NMe<sub>2</sub>) with 4-pyridyl substituents were previously reported to efficiently oxidize THF to 2-hydroxytetrahydrofuran (THF–OH).<sup>85</sup> Substrate (THF) oxidation was proposed as an “inner-sphere oxidation” because of a likely pre-equilibrium step involving THF binding to the copper–dioxygen adduct.<sup>89</sup> Also, in a detailed study conducted by Tolman and co-workers on the mechanism of formation for the  $\beta$ -diketiminate  $\text{Cu}^{\text{III}}\text{-}\eta^2\text{-O}_2^{2-}$  adduct, an associative oxygenation pathway (Scheme 6) involving THF coordination (pathway B) was proposed on the basis of comparisons to the same reaction in THF/MeCN mixtures (pathway A).<sup>13</sup> Complementary theoretical calculations led to a proposed transition state that involved dioxygen and solvent bound to copper simultaneously, either THF or MeCN accordingly.

**Proposed Mechanisms for O<sub>2</sub> Binding to the  $\text{D}^{\text{I}}\text{LCu}^{\text{I}}$  Complexes (D = NMe<sub>2</sub>, Im, Py).** In the present work and as described above, positive  $\Delta S^\ddagger$  values were measured for O<sub>2</sub> binding to  $^{\text{Im}}\text{LCu}^{\text{I}}$  ( $\Delta S^\ddagger = 35.1 \text{ J mol}^{-1} \text{ K}^{-1}$ ) and  $^{\text{NMe}_2}\text{LCu}^{\text{I}}$  ( $\Delta S^\ddagger = 80.1 \text{ J mol}^{-1} \text{ K}^{-1}$ ) in THF solvent, to the first approximation similar to that found for  $^{\text{Py}}\text{LCu}^{\text{I}}$  in EtCN but very different from that for  $^{\text{Py}}\text{LCu}^{\text{I}}$  in THF (and  $[\text{Cu}^{\text{I}}(\text{Me}_6\text{tren})]^+$  in EtCN) (see Table 3). Such a drastic difference in the O<sub>2</sub> binding mechanism depending on the variable N-donor moiety of  $\text{D}^{\text{I}}$  is surprising.

Scheme 7



Scheme 8

Smirnov and Roth:



Suggested Here:



We suggest changes in the electron distribution and/or coordination variations within the species upon O<sub>2</sub> ligation to Cu<sup>I</sup> are responsible, and it is not simply related to the order in which O<sub>2</sub> or solvent coordinate. More specifically, the transition-state differences may be largely based on whether Cu<sup>I</sup> → O<sub>2</sub> ET occurs before or after solvent dissociation, with the coordination of O<sub>2</sub> always being the initial step.

As shown in Scheme 7, the negative  $k_{\text{O}_2}$ -affiliated  $\Delta S^\ddagger$  value (associative mechanism) for  $^{\text{Py}}\text{LCu}^{\text{II}}\text{-O}_2^-$  in THF suggests a late transition state in which ET occurs before or concomitant with solvent release. Conversely, the positive  $k_{\text{O}_2}$ -affiliated  $\Delta S^\ddagger$  values (dissociative mechanism) for O<sub>2</sub> binding to  $^{\text{Im}}\text{LCu}^{\text{I}}$  in THF,  $^{\text{NMe}_2}\text{LCu}^{\text{I}}$  in THF, and  $^{\text{Py}}\text{LCu}^{\text{I}}$  in EtCN suggest an early transition state in which ET can occur only after solvent is released (see Scheme 7). Note that a computational analysis of the proposed mechanism has not been conducted, and therefore the proposed internal electron density distributions or solvent positioning (ligated or not) cannot be conclusively supported. However, the similarity of the dissociative processes for formation of the square pyramidal  $^{\text{NMe}_2}\text{LCu}^{\text{II}}\text{-O}_2^-$  species in THF and the trigonal bipyramidal  $^{\text{Im}}\text{LCu}^{\text{II}}\text{-O}_2^-$  and  $^{\text{Py}}\text{LCu}^{\text{II}}\text{-O}_2^-$  species in THF and EtCN (respectively) again points out that the reaction mechanism is not solely dependent on geometry or solvent medium, but rather the degree of solvent and/or O<sub>2</sub>-fragment interaction, i.e., electronic distribution within a given species.

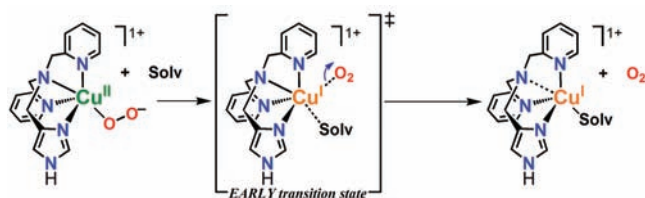
Smirnov and Roth have proposed a two-step, inner-sphere ET mechanism for the oxidation of O<sub>2</sub><sup>•-</sup> to O<sub>2</sub> by the copper(II) complexes of  $\text{PyL}$  and tris(2-pyridylethyl)amine (TEPA) in dimethylformamide (DMF)/THF mixtures.<sup>90</sup> Based on low-temperature stopped-flow kinetic experiments and competitive <sup>18</sup>O isotope effects, a pre-equilibrium step with formation of a Cu–O<sub>2</sub> species was suggested to occur prior to O<sub>2</sub> release (see Scheme 8). Formal oxidation states were not emphasized (Cu<sup>II</sup>–O<sub>2</sub><sup>•-</sup> versus Cu<sup>I</sup>–O<sub>2</sub>) for the intermediate species; therefore, an electrostatic versus covalent Cu–O<sub>2</sub> interaction was not designated. However, the release of O<sub>2</sub> was designated as the rate-determining step which would complete the overall ET process, i.e., reduction of the copper(II) ion. Formation of a pre-equilibrium complex is analogous to our proposal of a pre-

(89) Shearer, J.; Zhang, C. X.; Zakharov, L. N.; Rheingold, A. L.; Karlin, K. D. *J. Am. Chem. Soc.* **2005**, *127*, 5469–5483.

(90) Smirnov, V. V.; Roth, J. P. *J. Am. Chem. Soc.* **2006**, *128*, 3683–3695.

**Table 4.** Comparison of CO and O<sub>2</sub> Bimolecular Rates and Binding Constants at 298 K for Select Ligand–Copper(I) Complexes, Hemocyanins (Hc), and Selected Hemes

compound or protein	$K_{\text{CO}}$ (M <sup>-1</sup> )	$K_{\text{O}_2}$ (M <sup>-1</sup> )	$k_{\text{CO}}$ (M <sup>-1</sup> s <sup>-1</sup> )	$k_{\text{O}_2}$ (M <sup>-1</sup> s <sup>-1</sup> )	$k_{-\text{CO}}$ (s <sup>-1</sup> )	$k_{-\text{O}_2}$ (s <sup>-1</sup> )
NMe <sub>2</sub> LCu <sup>I</sup> (THF)	$4.9 \times 10^3$	100	$2.5 \times 10^9$	$2.3 \times 10^{11}$	$5.0 \times 10^5$	$2.3 \times 10^9$
Im <sup>+</sup> LCu <sup>I</sup> (THF)	$2.4 \times 10^3$	17.4	$2.8 \times 10^9$	$3.4 \times 10^{10}$	$1.1 \times 10^6$	$1.9 \times 10^9$
PyLCu <sup>I</sup> (THF)	$1.2 \times 10^4$	15.4	$1.9 \times 10^9$	$1.3 \times 10^9$	$1.6 \times 10^5$	$1.3 \times 10^8$
PyLCu <sup>I</sup> (CH <sub>3</sub> CN)	220	0.38	$5.9 \times 10^7$	$5.8 \times 10^7$	$2.7 \times 10^5$	$1.5 \times 10^8$
myoglobin (human)	$2.6 \times 10^7$	$(0.74\text{--}117) \times 10^4$	$7.6 \times 10^5$	$(1.4\text{--}25) \times 10^7$	0.022	22
hemoglobin (human)	$4.6 \times 10^8$	$(2.9\text{--}48) \times 10^5$	$4.6 \times 10^6$	$(2.9\text{--}22) \times 10^7$	0.009	13.1
Limulus Hc (arthropod)	$(2.7\text{--}11.2) \times 10^3$	$(2.6\text{--}5.4) \times 10^5$	$(2\text{--}4.3) \times 10^5$	$(1.3\text{--}1.9) \times 10^6$	38–75	2.4–7.5
Busycon Hc (mollusk)	$220 \times 10^3$	$1.8 \times 10^5$	$7.7 \times 10^5$	$(1.1\text{--}2.2) \times 10^6$	3–4	6.5–11.5

**Scheme 9**

electron-transfer intermediate step upon formation of  $^{\text{D}}\text{LCu}^{\text{II}}\text{-O}_2^-$  (Scheme 8).

**Temperature Dependence (193 vs 298 K) of Equilibrium O<sub>2</sub> Binding Constants ( $K_{\text{O}_2}$ ,  $\Delta H^\ddagger$ ,  $\Delta S^\ddagger$ ) and Dissociation Rates ( $k_{-\text{O}_2}$ ,  $\Delta H^\ddagger$ ,  $\Delta S^\ddagger$ ).** Dissociation of O<sub>2</sub> from  $^{\text{D}}\text{LCu}^{\text{II}}\text{-O}_2^-$  has an early transition state ( $+\Delta S^\ddagger$ ) for all species studied that involves the transfer of an electron from O<sub>2</sub><sup>•-</sup> to copper(II) followed by coordination of solvent (THF) and concomitant release of O<sub>2</sub>. This Cu–O<sub>2</sub> bond-breakage process is depicted for  $^{\text{Im}}\text{LCu}^{\text{II}}\text{-O}_2^-$  in Scheme 9. The  $k_{-\text{O}_2}$  activation parameters corresponding to  $^{\text{Im}}\text{LCu}^{\text{II}}\text{-O}_2^-$  are almost the same as those for  $^{\text{NMe}_2}\text{LCu}^{\text{II}}\text{-O}_2^-$ , suggesting the same O<sub>2</sub> release mechanism. However, for O<sub>2</sub> dissociation from  $^{\text{Py}}\text{LCu}^{\text{II}}\text{-O}_2^-$ , the corresponding activation parameters (Table 3) have slightly higher values than for the aforementioned species, suggesting a larger geometric change upon dioxygen loss.

The O<sub>2</sub> binding constants ( $K_{\text{O}_2}$ ) for all  $^{\text{D}}\text{LCu}^{\text{II}}\text{-O}_2^-$  complexes are of approximately the same magnitude ( $10^5 \text{ M}^{-1}$ ) at 193 K, overall favoring formation of the cupric–superoxo species. As expected, the equilibrium shifts more toward formation of the solvento species at 298 K. The  $K_{\text{O}_2}$  values clearly show the solvent effect, whereas compared to THF, EtCN significantly inhibits O<sub>2</sub> binding to  $^{\text{Py}}\text{LCu}^{\text{I}}$ . However, Me<sub>6</sub>TREN is a more Lewis basic ligand than is  $^{\text{Py}}\text{L}$ , such that O<sub>2</sub> binding to  $[\text{Cu}^{\text{I}}(\text{Me}_6\text{tren})]^+$  seems unaffected.

**Summary of 1:1 Cu/CO and Cu/O<sub>2</sub> Binding to  $^{\text{D}}\text{LCu}^{\text{I}}$  and Related 2:1 Cu/O<sub>2</sub> Complexes.** In the present study, CO, as a redox-inactive O<sub>2</sub> surrogate, was examined in its interactions with ligand–copper(I) complexes ( $^{\text{D}}\text{LCu}^{\text{I}}$ ). Data obtained concerning the CO binding kinetics and thermodynamics in THF were compared to those for 1:1 O<sub>2</sub> binding to  $^{\text{Py}}\text{LCu}^{\text{I}}$ ,  $^{\text{Im}}\text{LCu}^{\text{I}}$ , and  $^{\text{NMe}_2}\text{LCu}^{\text{I}}$ , where end-on ( $\eta^1$ ) coordination occurs. The formation of 1:1 Cu/O<sub>2</sub> adducts was *not* observed for  $^{\text{Q}}\text{LCu}^{\text{I}}$ ,  $^{\text{TB}}\text{P}^{\text{L}}\text{Cu}^{\text{I}}$ , and  $^{\text{Bz}}\text{LCu}^{\text{I}}$  under the same solution reaction conditions by laser flash photolysis of the CO adducts.<sup>91</sup> Since these cuprous complexes in fact do react with dioxygen to form 2:1 Cu/O<sub>2</sub> species under steady-state conditions,<sup>60,63,64</sup> it is likely that primary 1:1 Cu/O<sub>2</sub> binding does not compete kinetically (e.g.,  $\Delta A$  is too small) under the conditions employed, i.e., those used for all of the complexes examined in these studies.

In our previous reports,<sup>15,59</sup> the CO and O<sub>2</sub> binding kinetics of  $^{\text{Py}}\text{LCu}^{\text{I}}$  in THF solvent were detailed, with one finding being

that  $k_{\text{CO}} \approx k_{\text{O}_2}$  (Table 2). A look at the  $k_{\text{CO}}$  vs  $k_{\text{O}_2}$  values within Table 4, with data added in from the present study on  $^{\text{Im}}\text{LCu}^{\text{I}}$  and  $^{\text{NMe}_2}\text{LCu}^{\text{I}}$  (i.e., with one altered N-donor arm), gives the impression that these latter complexes have a very similar behavior. However, a significant finding in this report (Tables 3 and 4) is that there is a major change in the mechanism of O<sub>2</sub> binding to  $^{\text{Im}}\text{LCu}^{\text{I}}$  and  $^{\text{NMe}_2}\text{LCu}^{\text{I}}$  in THF; *the ligand binding occurs via dissociative rather than associative processes*. Recall that the dissociative mechanism *does occur* for both CO and O<sub>2</sub> binding to  $^{\text{Py}}\text{LCu}^{\text{I}}$  in the strong competing solvent EtCN. Electron transfer from copper(I) to O<sub>2</sub> seems the only factor possible to explain a change in mechanism. The CO binding behavior to the reduced copper(I) species for the  $^{\text{D}}\text{L}$  series is essentially the same (Tables 1 and 2). The (electrochemical study) derived  $E_{1/2}$  values for  $^{\text{Im}}\text{LCu}^{\text{I}}$  and  $^{\text{NMe}_2}\text{LCu}^{\text{I}}$  are the same but more negative than that for  $^{\text{Py}}\text{LCu}^{\text{I}}$ ; however, the coordination geometries of the copper(II) complexes of  $^{\text{Im}}\text{L}$  ( $\sim^{\text{Py}}\text{L}$ ) and  $^{\text{NMe}_2}\text{L}$  are different (*vide supra*). Thus, we conclude that the ET properties/kinetics of the O<sub>2</sub> interaction somehow lead to the change in mechanism observed. Solvent release is initiated by O<sub>2</sub> interaction with copper(I) (i.e., we suggest a Cu<sup>I</sup>–O<sub>2</sub> transient forms) *prior* to ET (Scheme 7), giving the observed  $^{\text{D}}\text{LCu}^{\text{II}}\text{-O}_2^-$  product. To summarize in other words, the reaction mechanism is governed by the order that ET from copper(I) to O<sub>2</sub> occurs; for  $^{\text{Py}}\text{L}$ , ET occurs before solvent is released, perhaps outer-sphere, but not so for  $^{\text{Im}}\text{L}$  or  $^{\text{NMe}_2}\text{L}$ . For  $^{\text{Im}}\text{L}$  and  $^{\text{NMe}_2}\text{L}$ , a dissociative interchange mechanism (*vide supra*) may be an appropriate description in which bond breaking (Cu<sup>I</sup>–solv) dominates over bond formation and ET (Cu<sup>I</sup> + O<sub>2</sub> → Cu<sup>II</sup>–O<sub>2</sub><sup>•-</sup>).

For all ligand–copper complexes studied,  $K_{\text{CO}}$  is much larger than  $K_{\text{O}_2}$ , primarily as a result of the lower CO dissociation rate constant ( $k_{-\text{CO}} < k_{-\text{O}_2}$ ). Breakage of the Cu–O<sub>2</sub> bond is more favorable than Cu–CO bond breakage, even though the former involves an ET step. The high  $k_{-\text{O}_2}$  values are a result of the highly favorable  $\Delta S^\ddagger$  value attributed to a late transition state (which leads to O<sub>2</sub> release) and the structural rearrangement that occurs upon redox changes.

As emphasized, the copper(II)– $\eta^1$ -superoxo species generated from  $^{\text{Py}}\text{LCu}^{\text{I}}$ ,  $^{\text{Im}}\text{LCu}^{\text{I}}$ , and  $^{\text{NMe}_2}\text{LCu}^{\text{I}}$  are spectroscopically very similar. In fact, spectroscopically (and therefore structurally) similar Cu/O<sub>2</sub> = 2:1 adducts also form, dicopper(II)– $\mu$ -1,2-(*end-on*)-peroxo species  $\{[(^{\text{D}}\text{L})\text{Cu}^{\text{II}}]_2(\text{O}_2^{2-})\}^{2+}$  analogous to the well-characterized case for  $^{\text{Py}}\text{L}$  (Scheme 10).<sup>8,61,62,65</sup> However, the conditions (i.e., temperature) under which the  $\{[(^{\text{D}}\text{L})\text{Cu}^{\text{II}}]_2(\text{O}_2^{2-})\}^{2+}$  complexes are observed, and/or their relative stability, varies significantly. Thus, reaction dynamics, i.e., kinetics and thermodynamics, governing each reaction step likely vary significantly, as observed in the present study on the Cu/O<sub>2</sub> = 1:1 adducts. For example, the peroxo species of  $^{\text{Im}}\text{L}$  (Figure 7A) can only be observed at  $-128$  °C in 2-methyltetrahydro-

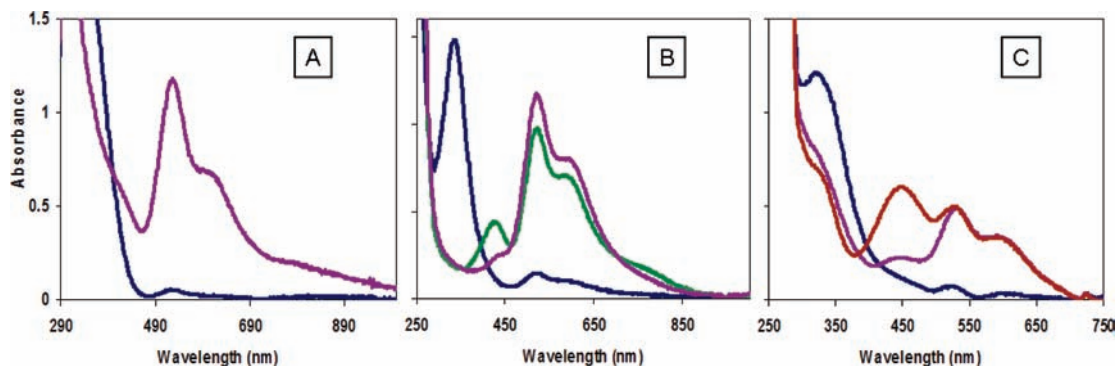
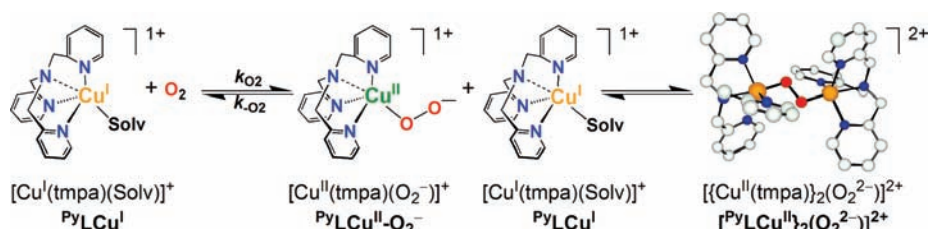


**Figure 7.** UV–visible spectra in MeTHF at  $-128\text{ }^{\circ}\text{C}$  representing  $\text{O}_2 + {}^{\text{D}}\text{LCu}^{\text{I}}$  (dark blue) to yield (A)  $\{[\text{Cu}^{\text{II}}(\text{tmpa})]_2(\text{O}_2^{2-})\}^{2+}$  (purple); (B)  $\text{PyLCu}^{\text{II}}\text{-O}_2^-$  (green) and  $\{[\text{PyL}(\text{Cu}^{\text{II}})]_2(\text{O}_2^{2-})\}^{2+}$  (purple); and (C)  $\{[\text{NMe}_2\text{L}(\text{Cu}^{\text{II}})]_2(\text{O}_2^{2-})\}^{2+}$  (purple) and a new copper–dioxygen adduct of  $\text{NMe}_2\text{L}$  (brown).

#### Scheme 10



furan (MeTHF).<sup>65</sup> In THF at  $-80\text{ }^{\circ}\text{C}$ , a Cu–O<sub>2</sub> intermediate is not observed.<sup>65</sup> Quite differently, formation of  $\text{PyLCu}^{\text{II}}\text{-O}_2^-$  can be detected on the benchtop in MeTHF at  $-128\text{ }^{\circ}\text{C}$  before complete conversion to the peroxo species (Figure 7B), which is stable for weeks at  $-80\text{ }^{\circ}\text{C}$  in THF.<sup>61</sup> Interestingly, for  $\text{NMe}_2\text{LCu}^{\text{I}} + \text{O}_2$ , a new, as-yet uncharacterized species is detected in MeTHF at  $-128\text{ }^{\circ}\text{C}$  in addition to the peroxo adduct (Figure 7C).<sup>76</sup> The new UV–vis feature(s) may suggest a different type or additional intermediate forms on the pathway to produce  $\{[\text{NMe}_2\text{L}(\text{Cu}^{\text{II}})]_2(\text{O}_2^{2-})\}^{2+}$ ; further studies are required.

**Comparison to Natural Copper and Heme Systems.** The kinetics and thermodynamics of CO and O<sub>2</sub> binding to the ligand–copper(I) complexes ( ${}^{\text{D}}\text{LCu}^{\text{I}}$ ) reported here are in line with studies carried out on natural and synthetic heme systems (Table 4). As said, carbon monoxide coordinates to the cuprous center ( ${}^{\text{D}}\text{LCu}^{\text{I}}$ ) with a higher affinity than that of O<sub>2</sub> ( $K_{\text{CO}} > K_{\text{O}_2}$ ), allowing for extension of the “flash-and-trap” experiment as inspired by extensive studies on a variety of heme systems. Furthermore, like our synthetic species,  $K_{\text{CO}}$  is much higher than  $K_{\text{O}_2}$  for the porphyrinate systems as a result of the lower CO dissociation rate ( $k_{-\text{CO}} < k_{-\text{O}_2}$ ); Cu–O<sub>2</sub> bond breakage is more favorable than breakage of the Cu–CO bond. The bimolecular rate constants for the copper complexes ( $k_{\text{CO}}$  and  $k_{\text{O}_2}$ ) are much higher than typically exhibited by heme systems, and the equilibrium binding constants are much lower. Therefore, the trends observed here are in line with conclusions drawn concerning gaseous small-molecule binding at the active site of the heme–copper heterobimetallic enzyme cytochrome *c* oxidase (CcO) (*vide supra*; see Introduction). In CcO, where one can imagine some competition for gases by both the heme and copper, CO coordinates to the Cu<sub>B</sub> site before thermally transferring to the Fe<sup>II</sup>-heme<sub>a3</sub> site (Figure 1). We have previously constructed a model binucleating iron and copper-containing ligand system as well as 1:1 heme/copper component systems that demonstrate this CO migration phenomenon, and most recently we have additionally examined NO transfer from iron to copper in the latter 1:1 component system.<sup>22,25</sup>

The interaction of CO and O<sub>2</sub> with hemocyanins (Hc) has also been extensively studied, and the characteristics are unlike

those of hemes. For Hc, lower equilibrium CO binding constants in comparison to O<sub>2</sub> ( $K_{\text{O}_2} > K_{\text{CO}}$ ) have been attributed to the higher rate of CO dissociation in comparison to that for O<sub>2</sub> ( $k_{-\text{CO}} > k_{-\text{O}_2}$ ) (see Table 4). This behavior most likely occurs because *both* copper(II) centers are involved in O<sub>2</sub> binding and release, whereas only one copper center binds CO; more structural rearrangements must occur in the release of O<sub>2</sub>. Conversely, the high O<sub>2</sub> association rates ( $k_{\text{O}_2}$ ) are a result of the 2:1 Cu/O<sub>2</sub> binding nature of the binuclear copper protein, a characteristic that is not exhibited upon CO binding (1:1 Cu/CO binding), *vide supra*.

As stated in the Introduction, an experiment such as the flash-and-trap experiment cannot be utilized for the binuclear copper proteins because  $K_{\text{O}_2} > K_{\text{CO}}$ . Laser flash photolysis has been used by Hirota et al. to examine O<sub>2</sub> binding by tyrosinase (Tyr) from *Streptomyces antibioticus*.<sup>44</sup> Following O<sub>2</sub> photoejection from oxy-Tyr to form deoxy-Tyr, re-formation of the starting dicopper(II)– $\mu$ - $\eta^2$ : $\eta^2$ -peroxo species was observed, while an initial 1:1 Cu/O<sub>2</sub> adduct was not detected. In a more recent study, Hirota, Bubacco, and co-workers reported thermodynamic data for oxygenation of Hc to form the dicopper(II)–(*side-on*)-peroxo species.<sup>45</sup> Interestingly, the values were comparable to those for the superoxo model compounds measured here, suggesting that formation of the 1:1 adduct is the rate-determining step and that oxyHc is easily produced through a nearly simultaneous two-electron-transfer step. This experimental finding fits with Solomon and co-workers’ prior computational studies on the O<sub>2</sub> binding process that occurs in Hc.<sup>92</sup>

#### Summary and Conclusions

In the present report, we have detailed the kinetics, thermodynamics, and coordination dynamics of 1:1 Cu<sup>I</sup>/CO and Cu<sup>I</sup>/O<sub>2</sub> binding within tetradentate ligand–copper(I) complexes with analogous coordination frameworks (Chart 2). The major findings are the following:

- (91) At much higher O<sub>2</sub> concentrations, the formation of a new Cu–O<sub>2</sub> adduct was observed and will be discussed in a different publication.  
 (92) Metz, M.; Solomon, E. I. *J. Am. Chem. Soc.* **2001**, *123*, 4938–4950.

1. In the ligand–copper(I) carbonyl complexes ( $^{\text{D}}\text{LCu}^{\text{I}}$ ), the variable N-donor arm of the synthetic ligand is dangling; all species possess the same four-coordinate core structure in solution where the cuprous ion binds to the bispicolylamine (PY1) tridentate chelate along with the CO molecule.

2. The fast kinetics of CO binding are measurably influenced by the exact nature of that uncoordinated donor arm. With change in ligand where  $K_{\text{CO}}$  increases,  $k_{\text{CO}}$  and  $k_{-\text{CO}}$  decrease;  $k_{-\text{CO}}$  decreases more substantially because the dangling donor ligand partially interacts (but to different extents) before it fully coordinates with the Cu(I) ion as CO dissociates.

3. In previous studies where the exact same PY1 ligand framework was present but with more-electron-releasing 4-pyridyl substituents,  $K_{\text{CO}}$  increased, as well as  $k_{\text{CO}}$ , very different from what was found here. In other words, ligand electronic variations previously led to the standard expected results, but here, (small) changes in the identity of D (the fourth donor, third ligand arm, Chart 1) led to a change in the relationship between  $K_{\text{CO}}$  and  $k_{\text{CO}}$ .

4. Using nanosecond laser flash photolysis to initiate gas ( $\text{CO}$ ,  $\text{O}_2$ ) reactions with copper(I) complexes, the unique finding of an extremely large rate constant for  $\text{O}_2$  binding, as previously described for  $^{\text{Py}}\text{LCu}^{\text{I}}$ , is shown to be a general phenomenon among D-PY1 ligand copper(I) complexes. Further, as seen before,  $k_{\text{O}_2}$  and  $k_{\text{CO}}$  values are quite similar to each other.

5. Changing one donor arm N-ligand from pyridyl to imidazolyl or to dimethylamino results in a change in the mechanism of  $\text{O}_2$  binding to the respective copper(I) complexes, associative for  $^{\text{Py}}\text{LCu}^{\text{I}}$  but dissociative for  $^{\text{Im}}\text{LCu}^{\text{I}}$  and  $^{\text{NMe}_2}\text{LCu}^{\text{I}}$ . We attribute this to aspects of the timing of ET from copper(I) to  $\text{O}_2$  as this molecule coordinates, in relation to the dissociation of the bound THF solvent molecule. Based on our other experiments, the change in mechanism is not simply related to a change in the  $^{\text{D}}\text{LCu}^{\text{III}}$  structures or the order in which  $\text{O}_2$  and THF coordinate.

6. The work discussed here establishes transient absorbance laser flash photolysis as an invaluable tool for determining fast, small-molecule ( $\text{CO}$  and  $\text{O}_2$ ) binding kinetics and thermodynamics of synthetic copper complexes such as  $^{\text{D}}\text{LCu}^{\text{I}}$ . Further, the ability to combine this utility with variable low-temperature control has enabled us to fully characterize 1:1 binding of  $\text{O}_2$

to  $^{\text{Im}}\text{LCu}^{\text{I}}$  and  $^{\text{NMe}_2}\text{LCu}^{\text{I}}$ , which was previously unobtainable with other relatively fast physical methods such as low-temperature stopped-flow kinetics/spectroscopy.

Overall, the results further support the general finding that subtle changes in coordination environment, as occurs over time through evolution in nature or through controlled ligand design in synthetic systems, can dictate the observed chemistry in terms of reaction kinetics, structure, and reactivity, and thus function. Many mononuclear and binuclear copper proteins exist that have an active-site ligation of three imidazolyl donors per copper center, yet they have very different functions, such as dioxygen transport in hemocyanin (Hc), dioxygen activation and phenol *o*-hydroxylation in tyrosinase (Tyr), electron transfer at the  $\text{Cu}_{\text{H}}$  site in peptidylglycine  $\alpha$ -hydroxylating monooxygenase (PHM) and/or dopamine  $\beta$ -monooxygenase, or  $\text{O}_2$  binding (and/or electron transfer) at  $\text{Cu}_{\text{B}}$  in cytochrome *c* oxidases (CcO) (see the Introduction). Therefore, gaining a deeper understanding of how the coordination environment and/or subtle changes in the surroundings influence the reactivity and/or binding properties of the copper center may help in understanding protein active-site ligand dynamics. Such information may also provide insight into secondary coordination sphere contributions that account for  $\text{N}_3\text{Cu}^{\text{I}}$  active-site functional differences.

**Acknowledgment.** We are grateful to the National Institutes of Health (K.D.K., NIH GM28962; G.J.M., NSF CHE0911558) for support of this research. We also acknowledge Drs. Amy A. Narducci Sarjeant and Maxime A. Siegler for relevant X-ray structural determination.

**Note Added after ASAP Publication.** This article was published ASAP on August 20, 2010, with incorrect versions of Figure 1, Charts 1 and 2, and Schemes 3, 7, and 9. The corrected version was reposted on August 27, 2010.

**Supporting Information Available:** X-ray data files (CIF); UV–visible data including spectrophotometric CO titrations, Van't Hoff plots,  $\Delta A$  spectra ( $\text{O}_2$  and CO binding), linear  $[\text{CO}]$  and  $[\text{O}_2]$  dependence, and Eyring plots. This material is available free of charge via the Internet at <http://pubs.acs.org>.

JA104107Q